Plasma-catalytic One-step Steam Reforming of Methane to Methanol: Revealing the Catalytic Cycle on Cu/MOR

*Yingzi Hao,[1#] Shangkun Li,[2 #] Wei Fang,[1#] Ximiao Wang,[1] Zhaolun Cui,[3] Kristof M. Bal,[2] Nick Gerrits,[2] Hongchen Guo,[1] Erik C. Neyts,[2] Annemie Bogaerts,[2] Yanhui Yi[1]**

[1]State Key Laboratory of Fine Chemicals, Frontier Science Center for Smart Materials, School of Chemical Engineering, Dalian University of Technology, Dalian 116024, P.R. China.

[2]Research group PLASMANT, Department of Chemistry, University of Antwerp, Universiteitsplein 1, BE-2610 Wilrijk-Antwerp, Belgium.

[3]School of Electric Power Engineering, South China University of Technology, Guangzhou 510630, China.

# These authors contributed equally.

Email: yiyanhui@dlut.edu.cn

KEYWORDS. methane conversion; plasma catalysis; anaerobic oxidation; methanol production;

ABSTRACT

Direct CH_4 to CH_3OH conversion is a long-standing grand challenge in catalysis. We present one-step steam reforming of methane to methanol (OSRMtM) by combining an atmospheric pressure $CH_4/H_2O/Ar$ plasma with a Cu/Mordenite (Cu/MOR) catalyst at 170 ^oC, achieving 77 % CH_3OH selectivity with 3.0 % CH_4 conversion. Catalyst characterization and plasma diagnostics, as well as D_2O and $H_2{}^{18}O$-labeled isotope tracer experiments reveal that the excellent reaction performance is attributed to Cu-O active sites confined by MOR zeolite. During plasma-catalytic OSRMtM, both CH_4 and H_2O are activated in the plasma and dissociated to produce radicals (CH_3, OH and H). These radicals drive the redox process between Cu^{2+} and Cu^{+}, playing an important role in plasma-catalytic OSRMtM. Although a gradual reduction of Cu^{2+} to Cu^{+} leads to slow deactivation of the Cu/MOR catalyst, the catalytic performance can be completely recovered through simple calcination, which enables a continuous plasma-catalytic OSRMtM process using a fluidized-bed reactor.

1. Introduction

Industrial CH_4 to CH_3OH conversion, shown in Figure 1 (black arrows), is energy-intensive and costly, motivating researchers to develop novel direct oxidation of methane to methanol (DOMtM) approaches.[1-3] CH_3OH protection is the key issue in DOMtM, because the produced methanol is not stable under the operative reaction conditions and might suffer over-oxidation to CO_2/CO.[4] Early studies by Periana and coworkers showed that electrophilic Hg and Pt complexes can oxidize methane in oleum, forming methyl hydrogen sulfate, which has to be hydrolyzed separately to release CH_3OH and SO_2.[5,6] Heterogeneous catalysts such as single-atom catalysts confined in 2D or 3D materials,[7,8] highly dispersed oxide clusters,[9,10] transition-metal (TM)-exchange zeolite,[11-13] and Au-Pd nanoparticle,[14-16] have also been proposed in combination with different oxidants (H_2O_2, N_2O, O_2) to realize DOMtM.

Compared to the above DOMtM routes, direct anaerobic oxidation of CH_4 to CH_3OH and H_2 is a strategy that "kills three birds with one stone": the conversion of CH_4 to CH_3OH, the production of green hydrogen without CO_2 emission (H_2O is a soft oxidant, which can avoid deep oxidation), and improved safety compared to the use of other oxidants (e.g., H_2O_2, N_2O, and O_2) in commercial setups when approaching the CH_4 explosion limit. Therefore, stepwise anaerobic oxidation of CH_4 to CH_3OH and H_2 has been proposed by Sushkevich et. al. using a chemical looping strategy.[17] Subsequently, Lee et al. observed the continuous generation of CH_3OH from CH_4 and H_2O on the Cu/MOR,[18] while Koishybay et al. found that oxygen in the methanol product mainly originates from H_2O, based on $H_2{}^{18}O$ isotope tracer experiments using a Cu-SSZ-13 catalyst.[19]

Although the direct anaerobic oxidation of CH_4 to CH_3OH and H_2 has broad prospects, it remains a topic of controversy.[20,21] First, oxidation of Cu^+ to Cu^{2+} by H_2O is thermodynamically unfavorable, and thus the catalytic cycle is difficult to be completed with H_2O as the sole oxidant.

Sun et al., studied the effect of O_2 (50 - 3000 ppm) on the performance of the CH_4/H_2O reaction system in a Cu-chabazite catalyst.[22] They showed that both H_2O and O_2 can be the oxygen source of hydroxyl in CH_3OH formation, and the introduction of trace O_2 in water plays an important role in driving the fast redox cycle of Cu^{2+}-Cu^{+}-Cu^{2+} to realize the continuous catalytic reaction of $CH_4/H_2O/O_2$ in order to produce CH_3OH and H_2. Moreover, the obtained CH_4 conversion (single pass) in all reported CH_4/H_2O reaction systems is extremely low (< 0.1%) for both the stepwise and the continuous reaction modes. Thus, one-step steam reforming of methane to methanol (OSRMtM) in continuous catalytic reaction mode with significant CH_4 conversion has not yet been achieved, and remains a challenge in catalysis.

Non-thermal plasma offers a potential avenue to activate molecules by energetic electrons instead of heat, which allows thermodynamically difficult reactions to occur at reduced temperatures.[23-26] Early studies showed that CH_3OH can be produced from a CH_4/H_2O dielectric barrier discharge (DBD) plasma, with 7.5 % CH_3OH selectivity at 50 % water-vapor concentration, where introducing a noble gas (Kr or Ar) can further enhance the CH_3OH yield.[27] Recently, a CH_4/H_2O DBD plasma reactor was also investigated to reveal the role of electron-induced chemistry and thermochemistry.[28] Plasma catalysis, which incorporates a catalyst into the plasma region, can further improve the conversion efficiency. Recently, a Cu/MOR catalyst was shown to exhibit improved performance in steam reforming of CH_4 for CH_3OH/H_2 production by plasma, with a reported selectivity of CH_3OH less than 30 % (86 % in liquid phase). Oxygen addition can avoid carbon deposition but also lead to CH_4 over-oxidation to CO_2.[29] Additionally, the Cu/MOR catalyst demonstrates improved performance than Cu/ZSM-5, Cu/MCM-41 and Cu/Beta in plasma-catalytic OSRMtM, attributing to the formation of oligomerized [Cu–O–Cu] species.[30] Based on above mentioned literature results, we can conclude that the selective synthesis

of CH_3OH by plasma-catalytic OSRMtM has not been realized with acceptable selectivity and conversion.

Herein, we combine a $CH_4/H_2O/Ar$ DBD plasma with a Cu/MOR catalyst to realize OSRMtM in continuous reaction mode. At 170 °C and atmospheric pressure, we achieve a 3.0 % CH_4 conversion (single pass) and 77 % CH_3OH selectivity without CO_2 production. Furthermore, we propose a clear redox catalytic cycle (Figure 1) driven by radicals, based on systematic characterization of the catalysts, plasma diagnostics, and isotope tracer experiment.

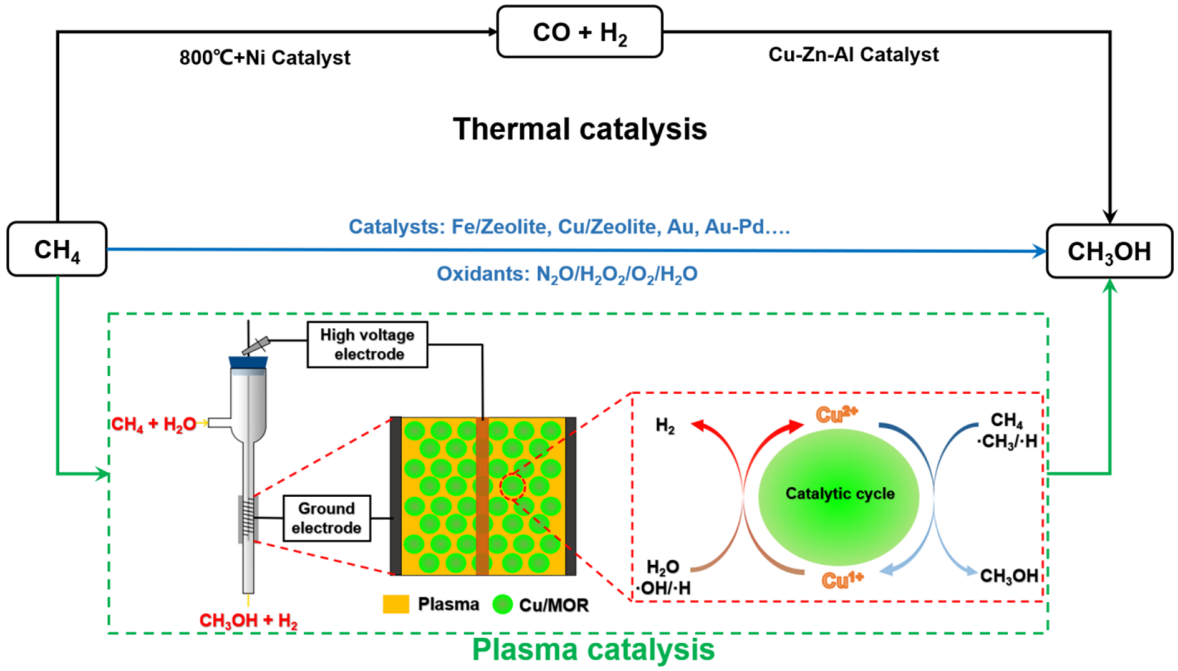

Figure 1. Schematic diagram of methane to methanol conversion: Commercial two-step process (black arrows), direct oxidation of methane to methanol (DOMtM) method (blue arrows), and our novel plasma-catalytic one-step steam reforming of methane to methanol (OSRMtM) approach (green arrow), with conceptual design for CH_3OH and H_2 production from CH_4 and H_2O through plasma catalysis.

2. Experimental section

2.1 Catalyst preparation

The catalyst was synthesized by the ion-exchange method. MOR (Mordenite, SiO_2/Al_2O_3=17) with weight of 50 g was added into 120 mL of 0.4 mol/L $Cu(NO_3)_2$ solution and stirred at 90°C for 2h in a water bath. The resulting suspension was filtered and extracted, then washed with 500 ml of deionized water. The process was repeated one to five steps to obtain different exchange levels of Cu/MOR. The Cu/MOR precursors were dried overnight in an oven at 100℃. Subsequently the samples were calcined in a muffle furnace at 500 °C for 5 h. The obtained samples are denoted as IE-1, IE-2, IE-3, IE-4, IE-5, corresponding to the different exchange steps of Cu/MOR.

2.2 *Plasma-catalytic setup*

The experimental setup is shown in Figure 2. The dielectric barrier discharge was generated in a cylindrical quartz tube (inner diameter of 9 mm, wall thickness of 2 mm). A stainless-steel rod installed in the quartz tube serves as an internal electrode, and the external electrode was an aluminum foil wrapped over the quartz tube. The diameter of the inner electrode is 2 mm and the discharge gap is 3.5 mm. The discharge length is 50 mm, as determined by the length of the aluminum foil wrapped around the quartz tube. The discharge gap was filled with catalyst particles (1.4 g, 20-40 mesh). CH_4 and Ar were monitored by a calibrated mass flow controller.

The gaseous products were analyzed by an on-line gas chromatograph (Tianmei GC-7900, TDX-01 column, alumina-filled column) equipped with a thermal conductivity detector (TCD) and a flame ionization detector (FID). Liquid products were collected by a cold trap (a mixture of isopropanol and liquid nitrogen at temperatures below -120°C) and then analyzed offline by GC-2014C (Shimadzu, polyethylene glycol-2000 column) and GC-MS (Agilent 5975C, DB-1701

column). The discharge frequency was fixed at 14.5 kHz and the discharge voltage was kept at about 2.5 kV. The discharge voltage and current were measured by a digital fluorescence oscilloscope (Tektronix, DPO 3012) with a high voltage probe (Tektronix P6015) and a current probe (Pearson 6585). The Lissajous plots represent the charge in the plasma as function of voltage, and the enclosed area denotes the average power consumed by the discharge, i.e., the product of energy consumed per cycle and the frequency of the cycle. A flow meter was used to measure the change in gas volume before and after the reaction, to account for gas expansion, needed to accurately calculate the conversion and product yields/selectivities.

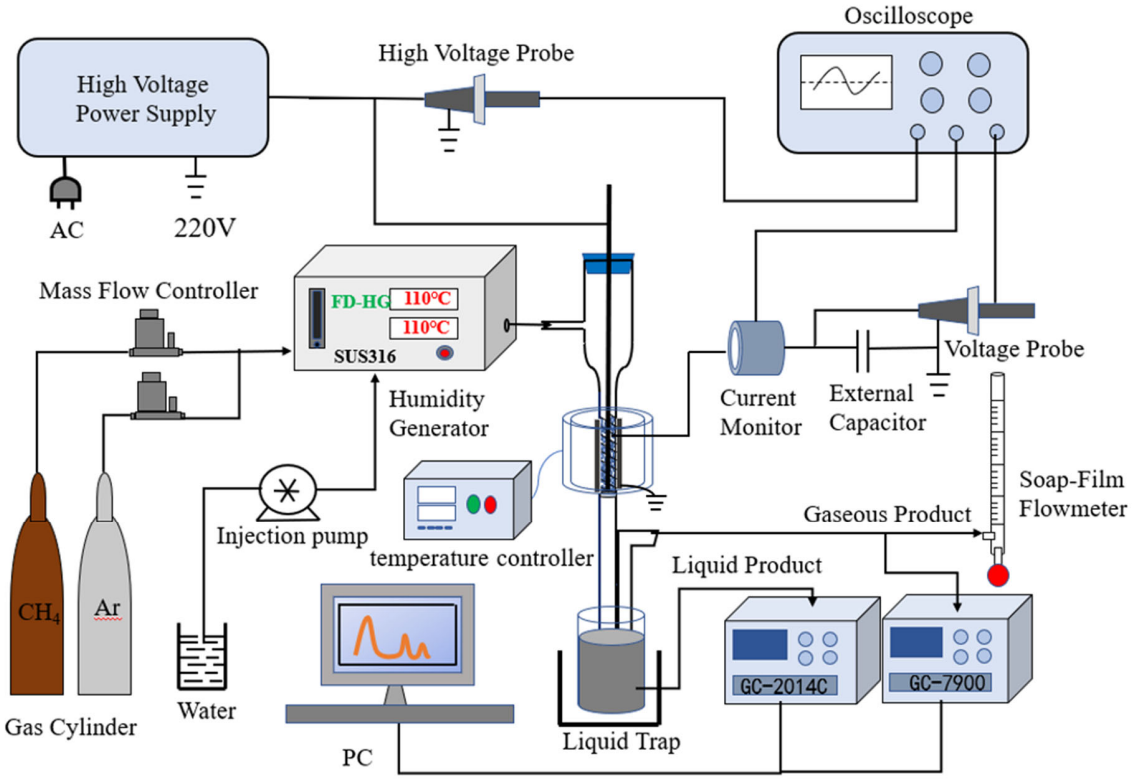

Figure 2. Schematic diagram of the experimental plasma-catalytic setup for plasma-catalytic OSRMtM.

We estimate the packing volume fraction of the catalyst bed using the drainage method. First, the amount of catalyst used to pack the discharge area is poured inside a measuring cylinder. Then, deionized water is slowly added by using a calibrated, adjustable volume pipette. This was done

until the catalyst was completely submerged and the water level reached the same volume as the discharge area of the reactor. The total volume of water added is used to determine the gas volume in the discharge region. In this case, the packing fractions of Cu/MOR are 0.8 ± 0.05.

The oxygenate products are analyzed offline using a cold trap to condense the liquid products, preventing overlap with large H_2O peaks in the online GC analysis. The calculations of conversion/selectivity remain accurate if only based on carbon-based, in case of low CH_4 conversion with negligible carbon deposition. The detailed calculation of conversion, product selectivity and energy efficiency are calculated by equations S1 ~ S10 in the SI, while the energy consumption of the process was defined by equation S11. All product concentrations were obtained by standard curves (Table S1).

2.3 Improvements on CH_4/H_2O plasma stability

H_2O can be activated by DBD plasma at room temperature, but low temperature might lead to non-uniformity mixing of CH_4 and H_2O and restrain the heat transfer in the fixed-bed to drive the endothermic OSRMtM reaction. To avoid the above mentioned problems in this study, we used a steam generator to supply water vapor, which was homogeneously mixed with CH_4 before passing through the plasma reactor. In addition, the gas line was heated with a heating ribbon, and the temperature was maintained at 115 ^oC to avoid condensation of the water vapor. The wall temperature of the DBD reactor (130, 170, 210, 250 or 290 ^oC) was maintained by a heating furnace. Also, noble gases (Ar) was added into the feed stock to ignite and stabilize the plasma because CH_4 and H_2O are both inert molecules. Ar is not consumed during the reaction process, and thus Ar can be recycled with the unreacted CH_4 to reduce the cost.

2.4 Catalyst characterization

The chemical composition of the Cu/MOR catalysts with different copper exchange steps was analyzed by X-ray fluorescence (XRF) on AXS Bruker's S8 TICER. N_2-physisorption was performed at -196°C on a Micromeritics ASAP 2020 instrument to obtain texture information. Prior to the measurements, the samples were degassed under vacuum at 400°C for 6 hours. The surface area was calculated by the Brunauer, Emmett and Teller (BET) method and the pore volume was obtained by the t-plot method. The crystal structures of Cu/MOR samples were measured by X-ray powder diffraction (XRD) using an X-ray diffractometer (Rigaku D-Max 2400) with Cu Kα radiation (λ = 0.15406 nm). We scanned data in the range of 5 to 80° in steps of 0.01 and at a scanning speed of 10 ºC/min. H_2-temperature programmed reduction (H_2-TPR) was performed on a Quanta chrome ChemBET Pulsar Chemisorption instrument. Prior to analysis, the samples (0.15 g) were pretreated with a helium flow from ambient temperature to 550 ºC for 60 min. Subsequently, the samples were cooled to 50 ºC in helium. Finally, H_2-TPR was carried out in a flow of a H_2/Ar mixture (120 ml/min, 10％ H_2). The temperature was increased from 50 ºC to 800 ºC with a heating rate of 10 ºC/min. Thermogravimetric analysis of the samples was performed by a Netzsch STA 449 F3 connected to a Balzers QMG 403D mass spectrometer. Prior to TG-MS analysis, 0.02 g samples were put in an alumina crucible and pretreated for 90 min at 110 °C. TG-MS experiments were carried out in an O_2/He mixture (20 % O_2) with a flow rate of 50 ml/min and a heating rate of 10 °C/min.

The catalyst acidity was tested by ammonia temperature-programmed desorption (NH_3-TPD) on a Quantachrome Chembet 3000 chemisorption apparatus. The sample pellets (0.15 g, 20-40 mesh) were loaded into a quartz U-shaped reactor and purged with helium for 1 h at 600 °C. Subsequently, the temperature was lowered to 373 K in order to adsorb ammonia for 30 minutes with a mixture of 5 % NH_3 in He. After adsorption, the sample was washed with a stream of helium

at 50 ml/min for 30 min to physically remove any adsorbed NH_3. Meanwhile, the desorption curve was recorded from 100 °C to 600 °C with a ramp rate of 17 °C/min. Infrared spectroscopy was carried out on a Nicolet 6700 infrared spectrometer with a scan range of 4000~400 cm^{-1} and a scan number of 64 steps. The catalyst samples (15 mg) were pressed into 15 mm self-supporting sheets in a stainless-steel mold and loaded into an IR cell with CaF_2. It was vacuumed to $3.5x10^{-3}$ Pa at 400 °C. After cooling to room temperature, the scanned spectrum was used as the background. Pyridine was adsorbed at room temperature for 30 min, then warmed up to 350°C for vacuum desorption for 30 min and cooled to room temperature to scan the spectrum.

X-ray photoelectron spectroscopy (XPS) was conducted by Thermo Fisher ESCALAB XI+ with Al Kα X-ray source. The C 1s binding energy value (284.8 eV) is used as an internal reference to calibrate the BE value. We present the XPS data of the copper (2p) region to provide information about the chemical environment of copper on the MOR framework. UV-Vis spectra were collected at 200-800 nm using an Agilent Cary 500 UV-Vis-NIR spectrophotometer with a diffuse reflectance integrating sphere attachment (built-in dra2500). Samples were taken with $BaSO_4$ as reference. High resolution transmission electron microscopy (HRTEM) was performed on JEM-2100F with an accelerating voltage of 200 kV.

2.5 Plasma diagnostics

The reactive plasma species in the CH_4/H_2O plasma were detected by optical emission spectroscopy (OES). The instrument model was an SP 2758 spectrometer from Princeton Instruments, USA, detection range: 200-1100 nm, slit width: 50 μm, exposure time: 1 s. The light is collected outside the reactor. In addition, the OH radicals produced in the plasma were detected by electron paramagnetic resonance (EPR) spectroscopy on a BRUKER E500 with central magnetic field of 335.5 mT, sweep width of 20 mT, sweep frequency of 9.423234 GHz, sweep

power of 6.325 mW, sweep resolution of 128000 points and at room temperature. 10 μL 5,5-dimethyl-1-pyrroline N-oxide (DMPO) as a spin trap was added to the collector, diluted with the aqueous solution collected during the 2 h reaction. A capillary tube was used to draw about 2 mL of the solution into the paramagnetic tube and the EPR test was performed at room temperature without light.

2.6 Isotope tracer experiment

To trace the origin of methanol and hydrogen formation by the plasma-catalytic OSRMtM process, we conducted isotope tracing experiments, by replacing the online GC with mass spectrometry (HIDEN) using SEM scanning mode. The Cu/MOR catalyst was initially heated at 540 °C to remove water before the experiment, and the Cu/MOR catalyst was purged with Ar at 170 °C for 30 min to avoid H_2O impacting the results. When using D_2O as an isotope tracing reagent, m/z signals of 3 (HD), 4 (D_2), and 33 (CH_3OD) were detected. By using $H_2{}^{18}O$ as the isotope tracing reagent, m/z signals of 31 (CH_3O) and 33 ($CH_3{}^{18}O$) were acquired. In each experiment, the feed gas was introduced into the discharge region and allowed to stabilize before initiating the discharge, and acquisition was terminated once the m/z signals stabilized.

3. Results and Discussion

3.1 Catalytic performance of OSRMtM

Figures 3A and 3B demonstrate that there is no chemical activity in the absence of plasma. In the case of $CH_4/H_2O/Ar$ plasma, liquid oxygenates can be obtained with a total selectivity of 64.7 %, and a CH_3OH selectivity of 28.0 %. The qualitative analysis of other liquid products can be found in Figure S1. After packing the MOR support in the plasma, the total liquid selectivity rapidly decreases, whereas the CH_4 conversion slightly increases. The hydrocarbon selectivities (i.e., C_xH_y) including C_2H_6, C_2H_4 and C_3H_8 are rapidly increased with the total selectivity of 58.7 %,

indicating C-C coupling reactions dominates on MOR support rather than CH_3OH production. When replacing the MOR zeolite by the Cu-exchanged MOR (Cu/MOR) catalyst, the total liquid selectivity rises sharply to 82.7 %, and the CH_3OH selectivity reaches 77 % with 3.0 % CH_4 conversion. In addition, after packing the plasma by Cu/MOR, the residence time of the feed gas was reduced into one fifth of the plasma only (the packing fractions of Cu/MOR is around 0.8 in the plasma). However, the CH_4 conversion was improved after packing Cu/MOR, further indicating catalytic role of Cu/MOR in promoting CH_4 conversion to produce CH_3OH.

We tested the Cu/MOR catalysts prepared by varying the number of Cu ion exchange steps. The CH_4 conversion and CH_3OH selectivity are gradually increased, and reach the peak by four steps of Cu ion exchange due to increased the Cu content on the MOR support. However, both the surface area and pore volume (Table S3) significantly decrease after five steps of Cu ion exchange, which may reduce the performance of OSRMtM (Figure 3C). Therefore, we here refer to Cu/MOR as the sample prepared through four steps of ion-exchange The reaction conditions, including temperature and CH_4/H_2O ratio, are also optimized (Figure S2). Optimal performance is reached at 170 ºC and a CH_4/H_2O ratio of 4:1. with a 77 % CH_3OH selectivity and 3.0 % CH_4 conversion. The energy consumption for CH_3OH production through plasma-catalytic OSRMtM by the Cu/MOR catalyst is 22.7 kJ/mmol (Figure S3), which is much lower than for plasma only (79.7 kJ/mmol) or for plasma + MOR (114.3 kJ/mmol). The above-mentioned results indicate the key role of the Cu/MOR catalyst in plasma-catalytic OSRMtM.

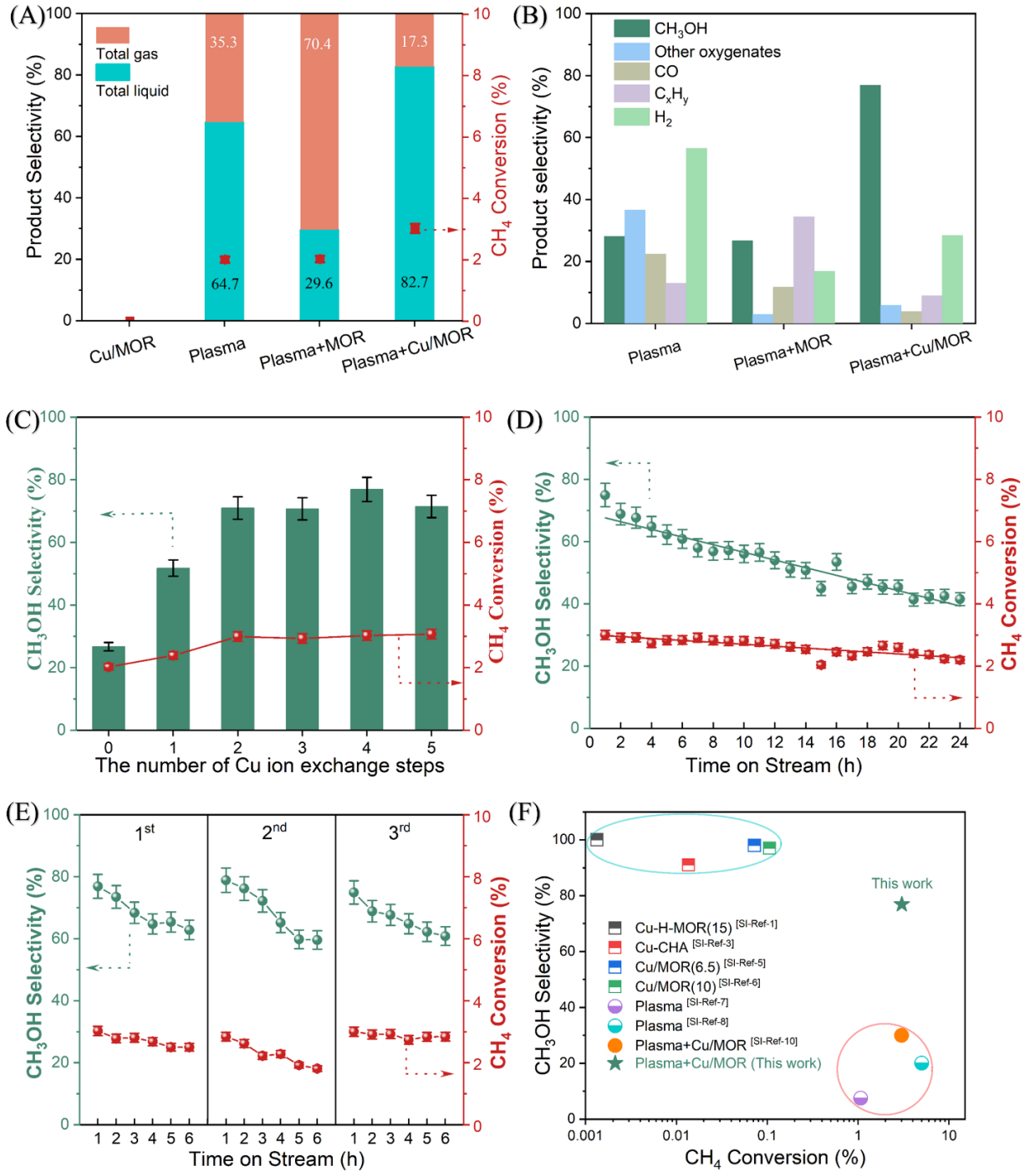

Figure 3. Experimental results of OSRMtM. (A) CH_4 conversion and total gas or liquid product selectivity (carbon-based) in the case of Cu/MOR catalyst only, plasma only, plasma + MOR support, and plasma + Cu/MOR catalyst; (B) Detailed gas and liquid selectivity; (C) Performance of Cu/MOR prepared by varying the number of Cu ion-exchange steps; (D) Stability test of plasma-catalytic OSRMtM for 24 h; (E) Catalyst

regeneration tests of spent Cu/MOR catalysts after calcination at 500 °C; (F) Comparison of our work with literature results using H_2O as oxidant, with detailed information in Table S2 of the Supporting Information (SI). The light blue and red circles indicate thermal and plasma (catalysis) experiments, respectively, showing a high selectivity but very low conversion, vs a reasonable conversion but very low selectivity, in contrast to this work. Reaction conditions: 1.7 wt.% Cu loading; CH_4: 20 ml/min; H_2O(g); 80 ml/min; Ar: 40 ml/min; discharge length: 5 cm; discharge power: 7 W; temperature of catalyst bed: 170 °C.

The catalytic stability of Cu/MOR for OSRMtM with 24 h continuous operation is shown in Figure 3D. Initially, 3.0 % CH_4 conversion and 77 % CH_3OH selectivity is achieved. However, the CH_3OH selectivity gradually declines from 77 % to 42 % after 24 h, and the CH_4 conversion slightly decreases from 3.0 % to 2.2 %, indicating that the Cu/MOR catalyst is gradually deactivating during the plasma-catalytic OSRMtM reaction. To explore the reason of this deactivation, the spent Cu/MOR catalyst (after 24 h reaction) was re-calcinated in air atmosphere, and then recovered to the original catalytic performance. The Cu/MOR sample was re-calcinated three times, and the catalytic performance could always be restored to that of the fresh catalyst (Figure 3E).

Finally, we compare our experimental results with reported OSRMtM results in literature in Figure 3F. The details are presented in Table S2 in the SI. The CH_3OH selectivities obtained by the chemical looping process are > 90 %, which is somewhat higher than our result (77 %). However, our CH_4 conversion (3.0 %) is at least an order of magnitude higher than those of the chemical looping process (< 0.1 %). Therefore, our plasma-catalytic OSRMtM process has great potential for CH_3OH production in a continuous flow reactor, i.e., a fluidized bed reactor, in which the Cu/MOR catalyst can be regenerated continuously through easy calcination.

3.2 Catalyst characterization

To reveal the role of the Cu/MOR catalyst in plasma-catalytic OSRMtM, we characterized the catalysts in detail. The XRD patterns of the Cu/MOR samples are shown in Figure 4A. These patterns exhibit the typical characteristics of a highly crystalline MOR phase, but the peaks of CuO, Cu_2O and Cu are absent. This means that Cu species were highly dispersed on the MOR, and that the lattice structure of the MOR was not disrupted during both catalyst preparation and catalytic tests. Figure 4B shows the H_2-TPR profiles of the Cu/MOR samples with different steps of ion-exchange. According to the literature,[31] the reduction of isolated Cu^{2+} species on a zeolite structure is usually achieved through a two-step mechanism, i.e., $Cu^{2+} + 1/2\ H_2 \rightarrow Cu^{+} + H^{+}$ and $Cu^{+} + 1/2\ H_2 \rightarrow Cu^{0} + H^{+}$. In the H_2-TPR profiles, two distinct peaks are indeed observed, in the range of 150-350 °C and 550-700 °C, respectively. The former peak is attributed to the reduction of isolated Cu^{2+} to Cu^{+}, while the latter peak is attributed to the reduction of Cu^{+} to Cu^{0}.[32] Furthermore, with increasing the number of ion-exchange steps, the former peak of H_2 consumption shifts towards the low temperature region, indicating more Cu-O species formation compared to the isolated copper species on the MOR during multiple ion exchange, which can be reduced by H_2 at a relatively low temperature. The texture and composition information on the Cu/MOR sample are summarized in Table S3 and Figure S4. The results show that the channels of the Cu/MOR are not destroyed after four-time Cu exchange. The HRTEM images (Figure S5) shows no evident copper particles on the Cu/MOR surface. Generally, several typical Cu-O species, i.e., such as di-copper ($[Cu_2(\mu\text{-}O)]^{2+}$, $[Cu_2(\mu\text{-}O)_2]^{2+}$, and bent $[Cu_2(\mu\text{-}O)_2]^{2+}$) and tri-copper ($[Cu_3(\mu\text{-}O)_3]^{2+}$, as indicated by experimental and modelling results from literature, can be formed in the channels and pores of the MOR.[11,33-36]

The acidity of the MOR and Cu-MOR samples was measured by NH_3 temperature programmed desorption (NH_3-TPD) and infrared spectroscopy of pyridine adsorption (Py-IR). The NH_3-TPD

profile (Figure S6) shows the central temperature of weak acidic sites shifts to lower temperatures after increasing the number of Cu ion-exchange steps, indicating weakening of the acidic strength.[37] The Py-IR (Figure 4C) results show two peaks at 1540 cm^{-1} and 1450 cm^{-1}, which can be ascribed to Brønsted and Lewis acidic sites, respectively. The amount of Lewis acidic sites increases with increasing number of ion-exchanges, which indicates that Cu^{2+} is present as Lewis acid by replacing H atoms of MOR catalyst.

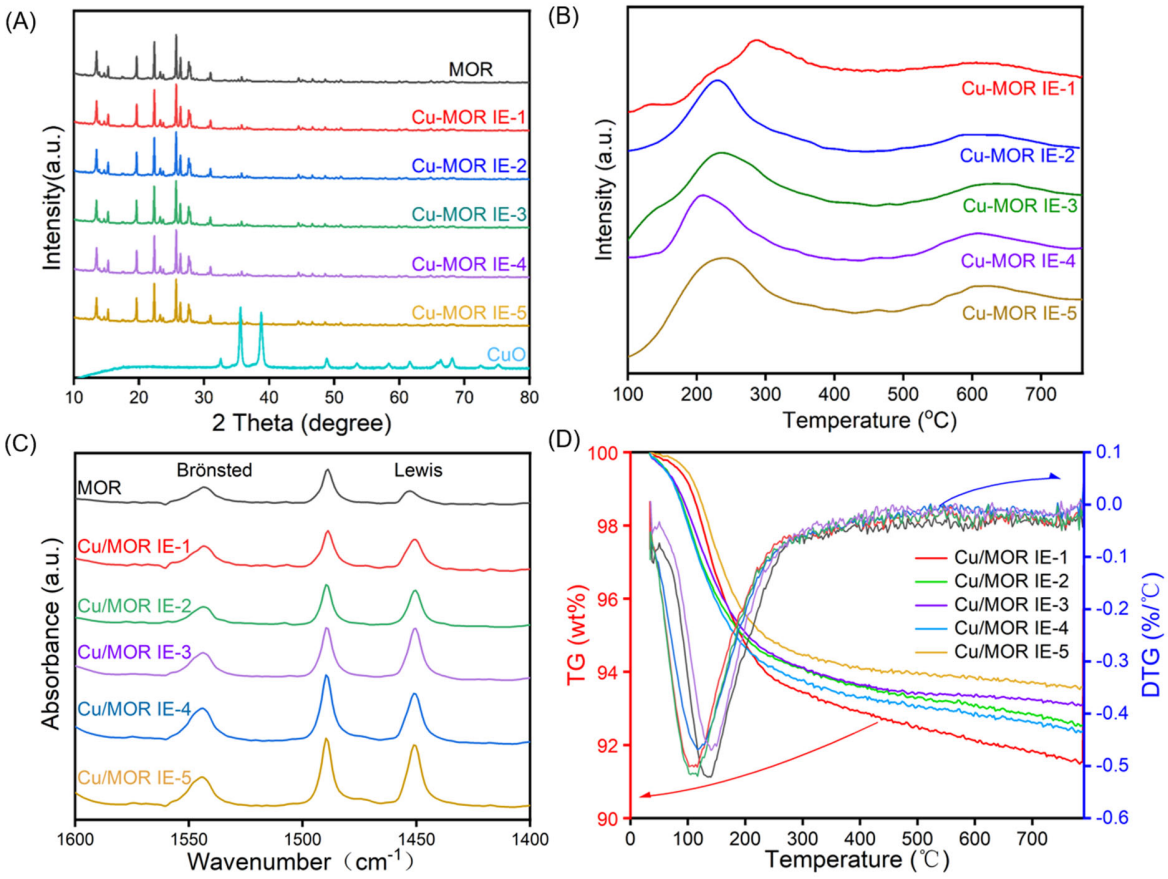

Figure 4. Characterization of the Cu/MOR catalyst of the fresh Cu/MOR catalysts prepared with a different number of ion-exchange steps. (A) XRD patterns; (B) H_2-TPR profiles; (C) Infrared spectroscopy patterns; (D) TG-MS patterns.

Furthermore, we characterized the spent Cu/MOR catalysts by thermogravimetric mass spectrometry (TG-MS, Figure 4D), and we measured very limited carbon deposition. The weight lost between 100-200 °C comes from water.[38] First order differentiation of the weight loss curves for the spent Cu/MOR catalyst shows that there is only one peak between 100-200 °C, indicating that the carbon accumulation in the reaction process is negligible. In general, the reasons of catalyst deactivation include poisoning, carbon deposition and sintering.[39] The purity of the feed gas used in the reaction process is 99.99%, which can help prevent poisoning of the Cu/MOR catalysts by impurities. In addition, the calcination temperature for preparing the catalyst is 540 °C, while the reaction temperature is only 170 °C, indicating that the sintering of Cu species on MOR is unlikely under the reaction conditions.

It should be mentioned that in the chemical looping process there is a redox reaction for converting CH_4 to CH_3OH.[17] Hence, it is reasonable to speculate that the main reason for the gradual deactivation of the Cu/MOR catalyst during our stability test may be a gradual reduction of Cu^{2+} active centers, because the reaction atmosphere not only contains a large amount of CH_4, but also produces abundant H_2, capable of reducing Cu^{2+} to Cu^{+} under NTP conditions. Thus, we designed three sets of experiments (Figure S7) to demonstrate the above scientific hypothesis: (A) A fresh Cu/MOR sample was placed on the catalyst bed, and Ar flow was used to purge the catalyst bed at room temperature for 30 min. After that, a CH_4/Ar/H_2O mixture replaced the Ar and the plasma was turned on to maintain the plasma-catalytic OSRMtM reaction for 3 h, 6 h or 9 h; (B) A fresh Cu/MOR sample was again placed on the catalyst bed, and an Ar flow was used to purge the catalyst bed at room temperature for 30 min. After that, a CH_4/Ar mixture replaced the Ar and the plasma was turned on to maintain the treatment for 20 min, 30 min or 40 min. (C) After 40 min CH_4 plasma treatment, the Cu/MOR sample was purged with an Ar flow at room temperature for

30 min. After that, a H_2O/Ar gaseous mixture replaced the Ar, and the plasma was turned on to maintain the treatment for 3 h, 6 h or 9 h. Finally, the above samples were characterized by X-ray photoelectron spectroscopy (XPS) and Ultraviolet–visible spectroscopy (UV-Vis), as shown in Figure 5.

For the Cu 2p results of the Cu/MOR samples, the XPS peaks at 933.5 eV and 936.3 eV are attributed to Cu^{2+} (with a satellite peak at 943.5 eV), while the XPS peak at 932.5 eV is attributed to Cu^{+} or Cu^{0}.[40] Furthermore, the XPS peak at 933.5 eV corresponds to the Cu^{2+} ion coordinated to the zeolite framework oxygen, and the peak at 936.3 eV includes mono(μ-oxo) di-copper, bis(μ-oxo) di-copper, tri-copper species, and Cu-OH^{+}.[41] As shown in Figure 5A, for the Cu/MOR samples that were used for the 3, 6 and 9 h plasma-catalytic OSRMtM reaction, we observe a significant increase of the Cu^{+} peak intensity but an obvious decrease of the Cu^{2+} intensity, compared with the fresh Cu/MOR sample. In addition, similar results were obtained for the Cu/MOR sample treated by the CH_4/Ar plasma for a much shorter time (Figure 5B). Furthermore, for the Cu/MOR sample after 40 min of treatment by CH_4/Ar plasma, the H_2O/Ar plasma treatment obviously increases the relative intensity of Cu^{2+} but lowers the relative intensity of the Cu^{+} peak (Figure 5C). The above XPS results demonstrate that CH_4 in the CH_4/Ar/H_2O plasma exhibits a strong reducing character, while H_2O exhibits a weak oxidizing character. In addition, the CH_4/Ar plasma shows a stronger reducing character than the CH_4/Ar/H_2O plasma, because the former needed a much shorter treatment time for the same effect (i.e., 20, 30 and 40 min, vs 3, 6 and 9 h), which suggests that the reduction of Cu^{2+} species during the plasma-catalytic OSRMtM reaction is mainly caused by the reducing character of CH_4 in the plasma.

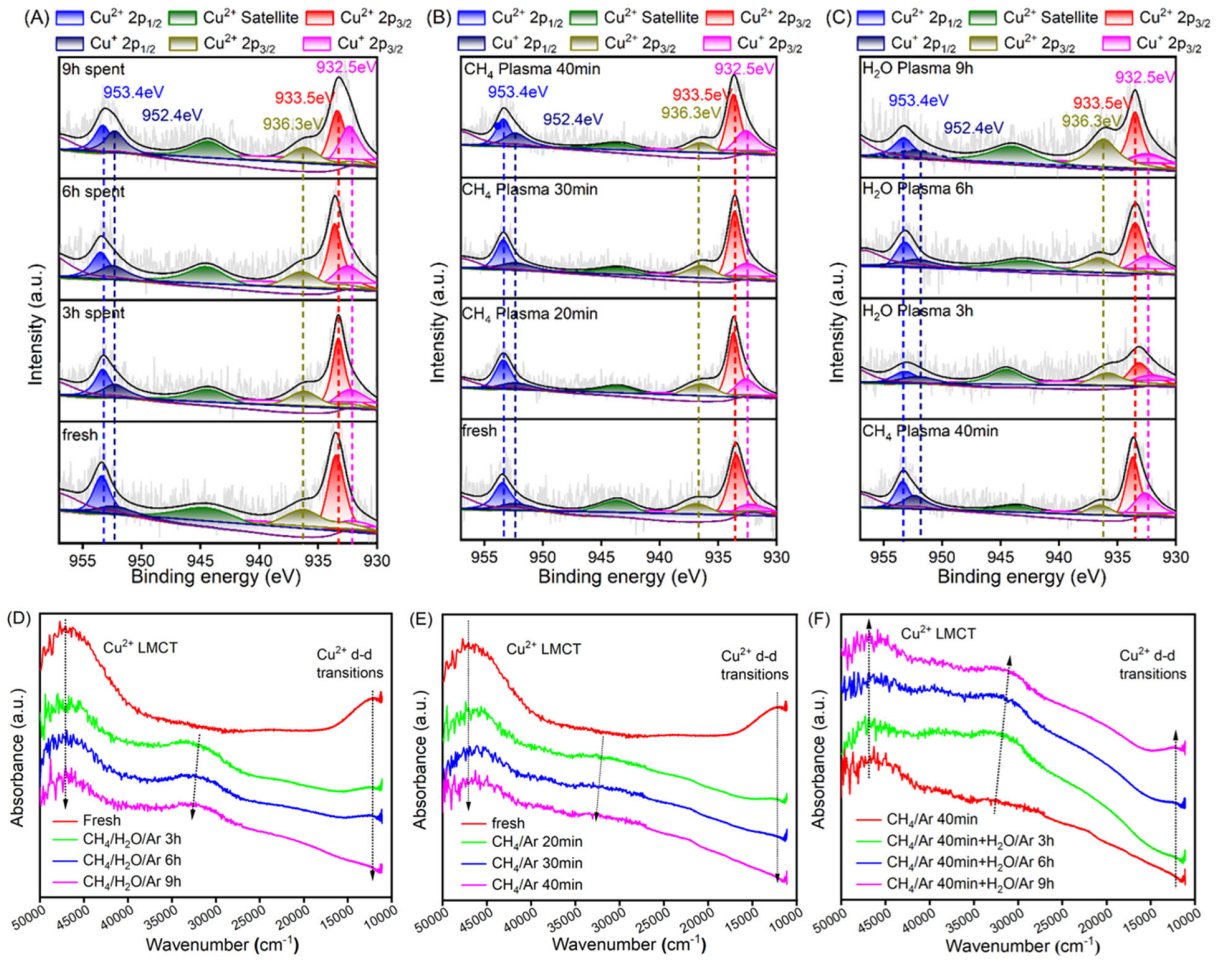

Figure 5. XPS spectra of Cu/MOR catalyst after plasma treatment under different conditions: (A) $CH_4/H_2O/Ar$ plasma; (B) CH_4/Ar plasma; (C) 40 min CH_4/Ar plasma followed by H_2O/Ar plasma; UV-Vis spectra of Cu/MOR after plasma treatment under different conditions: (D) $CH_4/H_2O/Ar$ plasma; (E) CH_4/Ar plasma; (F) 40 min CH_4/Ar plasma followed by H_2O/Ar plasma.

Dynamic changes of Cu/MOR were also investigated by Ultraviolet–Visible spectroscopy (UV-Vis, Figure 5D-F) for the above three experiments. A weak absorption peak at 12200 cm^{-1} corresponds to the d-d transition of the hydrated monomer Cu^{2+} ($3d^9$) with distorted octahedral coordination.[22,42,43] Electronic spectroscopic analysis involving the d-d leap is only applicable to Cu^{2+} ($3d^9$) since the Cu^+ ion has a fully occupied d-shell layer ($3d^{10}$).[44] Additionally, ligands to metals charge transfer (LMCT) for isolated Cu^{2+} ($O^{2-}Cu^{2+} \rightarrow O^{-}Cu^{+}$) between 40,000 cm^{-1} and

50,000 cm^{-1} are also observed.[22,42,43] Compared to the fresh catalyst, the catalyst treated by plasma shows a new absorption peak at 33000 cm^{-1}, which corresponds to the $Cu_3(\mu\text{-}O)_3$ species.[33] Moreover, prolonging the reaction time (Figure 5D) and treating the catalyst with CH_4/Ar plasma with different duration (Figure 5E) results in a significant decrease in the intensity of the spectral bands at 12200 cm^{-1}, 33000 cm^{-1} and 47000 cm^{-1}, indicating a continuous reduction of Cu^{2+}. However, the intensity of the spectral bands at 12200 cm^{-1} and 47000 cm^{-1} increases after H_2O/Ar plasma treatment (Figure 5F), indicating that Cu^+ can be oxidized to Cu^{2+}, which agrees with the XPS results. Interestingly, we found that it took around six hours for the H_2O/Ar plasma treatment to recover the intensity of the absorption peak at 12000 cm^{-1} when the Cu-MOR catalyst was treated by the CH_4/Ar plasma for 40 min, suggesting that the oxidizing character of the H_2O/Ar plasma is not strong enough.

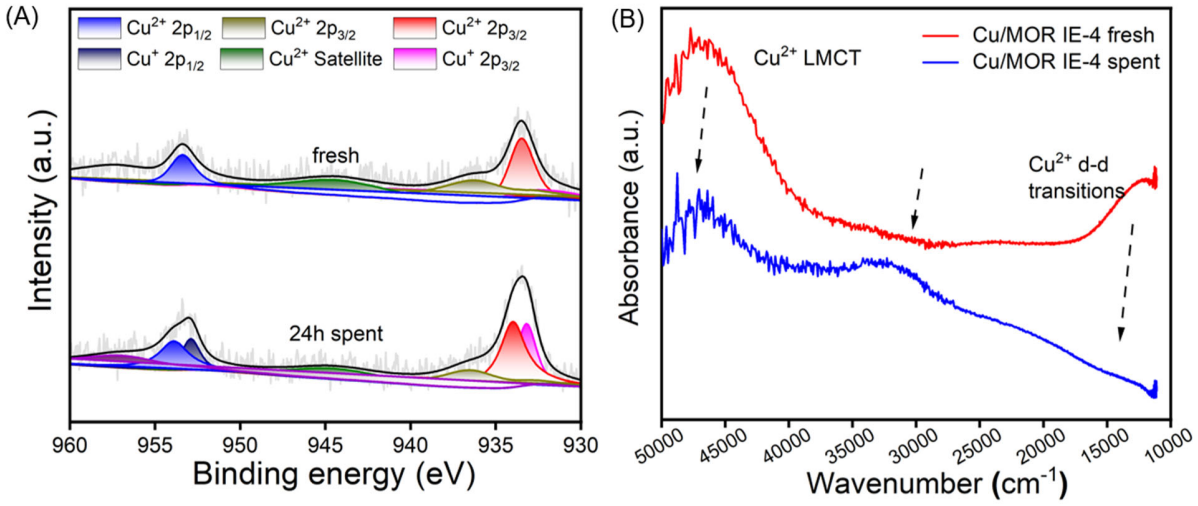

Figure 6. The characterization results of (A) XPS and (B) UV-vis, of fresh Cu-MOR and spent Cu-MOR after 24 h plasma-catalytic OSRMtM reaction

Indeed, the characterization of the spent Cu/MOR sample after 24 h continuous plasma-catalytic OSRMtM reaction demonstrates an obvious reduction of Cu^{2+} to Cu^+ species (Figures 6A and 6B). Therefore, the reduction of Cu^{2+} to Cu^+ species is faster than the oxidation of Cu^+ to Cu^{2+} species,

resulting in a net reduction of Cu^{2+} to Cu^{+}, which explains why the Cu/MOR catalyst gradually deactivates during the plasma-catalytic OSRMtM reaction. In other words, the oxidizing character of H_2O in the plasma is not strong enough to drive the continuous plasma-catalytic OSRMtM reaction with stable catalytic activity and selectivity. Fortunately, the Cu/MOR catalyst can be regenerated continuously through an easy calcination process, which enables a continuous plasma-catalytic OSRMtM process in a fluidized-bed reactor.

3.3 Reactive species diagnostics and isotope tracer experiment

Non-thermal plasma, capable of activating inert molecules through inelastic collisions with energetic electrons, provides new possibilities for CH_4 conversion.[45-48] Our experimental results demonstrate that the plasma-catalytic OSRMtM process can be realized by using a Cu/MOR catalyst at 170 °C and atmospheric pressure. In order to reveal the reaction mechanism, we investigated the active species by optical emission spectroscopy (OES) and electron paramagnetic resonance (EPR), as well as isotope tracer experiments.

Figure 7A shows the OES results. Because the light signal is collected outside the reactor, where there is a weak air discharge, N_2 and O signals appear. Notably, we collected spectral lines of CH (431.4 nm and 434 nm), H (656.3 nm) and OH (308 nm) radicals. CH radicals are usually generated by the stepwise dehydrogenation of CH_4, i.e., $CH_4 \rightarrow CH_3 \rightarrow CH_2 \rightarrow CH$, and the probability of generating CH_3, CH_2 and CH radicals was estimated to be 79 %, 15 % and 5 %, respectively.[43,46,47] Therefore, the OES signals of the CH radicals indicate that CH_3 radicals should be abundant in the CH_4/H_2O plasma. The appearance of spectral lines of OH radicals proves that H_2O is dissociated to form OH radicals in the $CH_4/Ar/H_2O$ plasma.

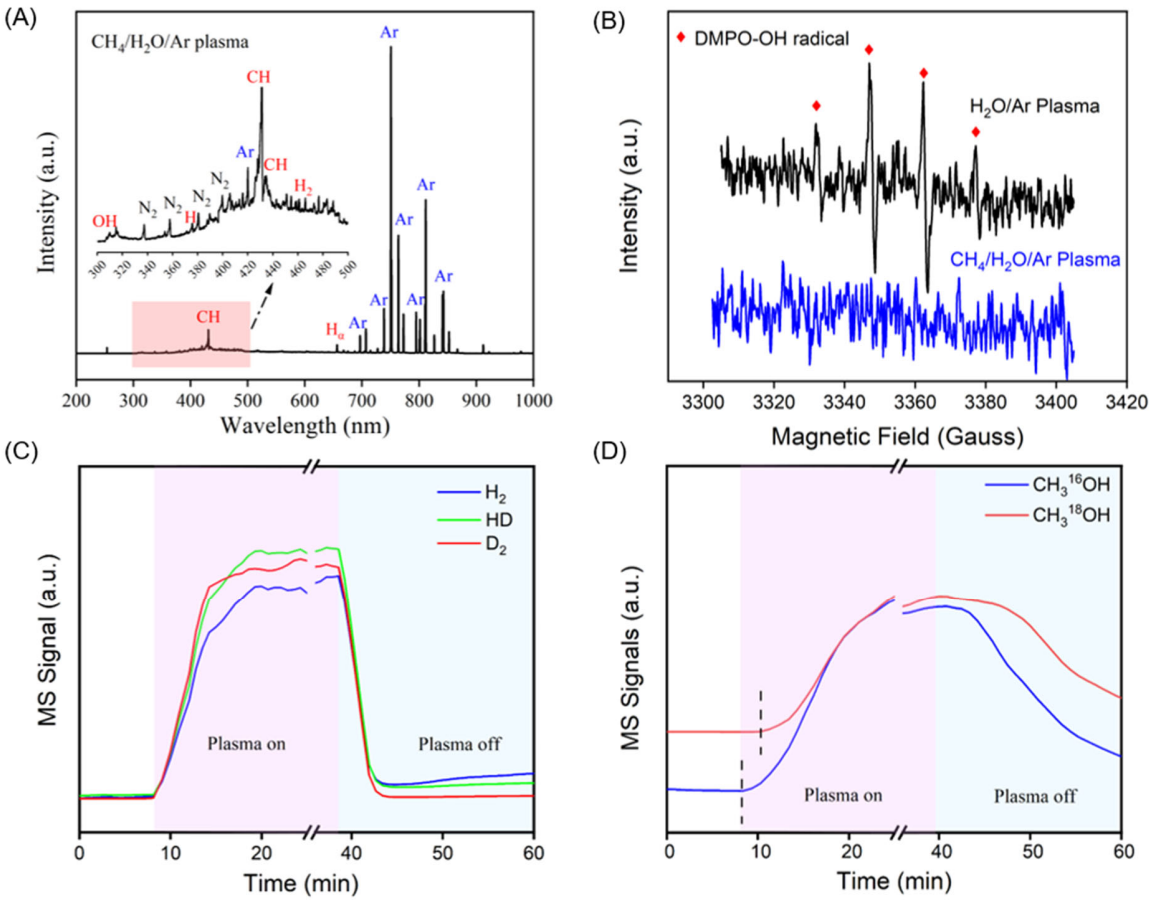

Figure 7. (A) Optical emission spectra of $CH_4/H_2O/Ar$ plasma with enlarged scale from 300 nm to 500 nm. (B) Electron paramagnetic resonance spectra, showing radicals in H_2O/Ar plasma and $CH_4/H_2O/Ar$ plasma, with DMPO added to the reaction mixture as the radical trapping agent. (C) Online mass spectral responses for unlabeled H_2 (m/z =2), labeled HD (m/z = 3) and D_2 (m/z = 4) in the plasma-catalytic OSRMtM process using D_2O as an isotope tracing reagent. (D) Online mass spectral responses for unlabeled methanol ($CH_3{}^{16}OH$, m/z =31) and ^{18}O-labeled methanol ($CH_3{}^{18}OH$, m/z = 33) using $H_2{}^{18}O$ as an isotope tracing reagent in the plasma-catalytic OSRMtM process.

We also carried out electron paramagnetic resonance (EPR) studies to detect radical species produced from the plasma. We selected 5,5'-Dimethyl-1-pyrroline-N-oxide (DMPO) as a radical trap in $CH_4/H_2O/Ar$ plasma and H_2O/Ar plasma, as shown in Figure 7B. For the EPR spectra of $CH_4/H_2O/Ar$ plasma, we do not observe peaks of $CH_3\cdot$ or $\cdot OH$ radicals. However, we observe an

obvious ·OH radical signal for the spectra of H_2O/Ar plasma.[15] This result further demonstrates that H_2O is dissociated to form ·OH radicals in the plasma, consistent with the OES results. The absence of ·OH radicals in the CH_4/H_2O/Ar plasma might be caused by the rapid reaction of ·OH with CH_3·to form CH_3OH.

Finally, we performed isotope tracing experiments during the plasma-catalytic OSRMtM reaction, and we used online mass spectrometry (MS) to detect the products. As shown in Figure 7C, H_2, HD, and D_2 were detected when using D_2O as an isotope tracing reagent (CH_4/Ar/D_2O plasma reaction), and three signals simultaneously rise, with decreasing intensity trend HD > D_2 > H_2, when the plasma is switched on. These results indicate the generated hydrogen comes from both H_2O and CH_4 during plasma-catalytic OSRMtM. As shown in Figure 7D, by using $H_2{}^{18}O$ as an isotope tracing reagent (CH_4/Ar/$H_2{}^{18}O$ plasma reaction), signals of two methanol molecules, i.e., $CH_3{}^{16}OH$ and $CH_3{}^{18}OH$, were acquired. However, the signal of $CH_3{}^{18}OH$ is delayed for around 3 min with respect to the $CH_3{}^{16}OH$ signal after plasma-on, indicating that the methanol production is mainly caused by surface reaction between oxygen species from Cu/MOR and CH_4 plasma-produced species (such as CH_3·). In addition, the intensity of the $CH_3{}^{18}OH$ signal gradually rises and eventually it becomes higher than that of $CH_3{}^{16}OH$, which means that ^{18}O from $H_2{}^{18}O$ gradually dominates the surface oxygen species on the Cu/MOR with time on stream. Furthermore, after switching the plasma off, the $CH_3{}^{16}OH$ signal immediately drops, while the $CH_3{}^{18}OH$ signal decreases slowly. This suggests that most of the active oxygen species inside the pores of Cu/MOR are gradually replaced by ^{18}O from $H_2{}^{18}O$ during the CH_4/Ar/$H_2{}^{18}O$ plasma reaction, and thus the produced methanol in the pore is dominated by $CH_3{}^{18}OH$, which needs more time to desorb from the pores into the gas phase.

To sum up, the Cu-O species confined by the framework of the MOR zeolite can be formed using the ion-exchange method, which can significantly improve CH_3OH production on plasma-catalytic OSRMtM. On the one hand, the zeolite-confined Cu-O species can significantly improve the adsorption of radicals (i.e., CH_3, H, and OH) generated by the plasma, indicated by the results of EPR and isotope tracing experiments. On the other hand, these radicals produced from plasma can also change the property of Cu/MOR catalyst. By designing three sets of experiments, we investigate the dynamic changes of Cu/MOR catalyst treated by CH_4/Ar/H_2O plasma, CH_4/Ar plasma, and H_2O/Ar plasma. Interestingly, we found there is a catalytic cycle from Cu^{2+} to Cu^{+} between CH_4/H_2O/Ar plasma and Cu/MOR catalyst, which is involved in plasma-catalytic OSRMtM process, as shown in Figure 1. The catalytic cycle driven by reactive radicals generated by plasma enables the reaction to occur at lower temperatures, offering a new pathway for CH_3OH production through plasma catalysis. However, the low CH_4 conversion is indeed the limitation of plasma-catalytic OSRMtM in this work. Thermodynamically, CH_3OH is not a favourable product, as CO and CO_2 are more stable. High temperature or high specific energy input can improve CH_4 conversion, but will also result in over-oxidation of CH_3OH. Future efforts will aim to enhance the yield of CH_3OH by further optimizing plasma parameters and catalytic active sites.

4. Conclusion

We demonstrated that the one-step anaerobic oxidation of methane to methanol by combining CH_4/H_2O/Ar plasma with a Cu/MOR catalyst at 170 °C and atmospheric pressure can achieve 77 % CH_3OH selectivity with 3.0 % CH_4 conversion. The energy consumption of plasma catalysis by Cu/MOR was reduced compared to plasma alone, from 79.7 kJ/mmol to 22.7 kJ/mmol. The excellent reaction performance is attributed to Cu-O active sites confined by the MOR zeolite. As indicated by our XPS and UV-Vis results, there is a catalytic cycle from Cu^{2+} to Cu^{+} between

CH_4/H_2O/Ar plasma and the Cu/MOR catalyst. Due to insufficient oxidizing ability of the H_2O plasma, we observed a slow deactivation of the Cu/MOR catalyst, which can however be recycled by calcination. Plasma diagnostics of the reactive species and isotope tracer experiments suggest that CH_4 and H_2O are dissociated in the plasma and the main radicals include CH_3, OH and H. This work presents a potential new technology for direct CH_4 to CH_3OH conversion by plasma catalysis and provides the practical insight in the mutual interactions between plasma and zeolite-confined catalysts.

ASSOCIATED CONTENT

Supporting Information. The Supporting Information is available free of charge at https://pubs.acs.org/xxx.

AUTHOR INFORMATION

Corresponding Author

*Yanhui Yi − State Key Laboratory of Fine Chemicals, School of Chemical Engineering, Dalian University of Technology, Dalian 116024, P. R. China

Author Contributions

The manuscript was written through contributions of all authors. All authors have given approval to the final version of the manuscript.

Author Contributions

Y. Hao., S. Li and W. Fang contributed equally to this paper. The manuscript was written through contributions of all authors. All authors have given approval to the final version of the manuscript.

Notes

The authors declare no competing financial interest.

ACKNOWLEDGMENT

Support of this work by the National Natural Science Foundation of China (No. 22272015). The China Scholarship Council is gratefully acknowledged (No. 202006060029). The research was also supported by the European Research Council (ERC) under the European Union's Horizon 2020 research and innovation programme (Grant Agreement No. 810182 – SCOPE ERC Synergy project).

REFERENCES

(1) Caballero, A.; Perez J., Methane as raw material in synthetic chemistry the final frontier. *Chem. Rev.* **2017**, 117 (13), 8497-8520.

(2) Li, S.; Ahmed, R.; Yi, Y.; Bogaerts A., Methane to methanol through heterogeneous catalysis and plasma catalysis. *Catalysts*, **2021**, 11, 590.

(3) Dummer, N.F.; Willock, D.J.; He, Q.; Howard, M.J.; Lewis, R.J.; Qi, G.; Taylor, S.H.; Xu, J.; Bethell, D.; Kiely, C.J.; Hutchings, G.J., Methane Oxidation to Methanol, *Chem. Rev.* **2023**, 123, 6359–6411.

(4) Blankenship, A.; Artsiusheuski, M.; Sushkevich, V.; van Bokhoven, J.A., Recent trends, current challenges and future prospects for syngas-free methane partial oxidation, *Nat. Catal.* 2023, 6, 748-762.

(5) Periana, R. A., Taube, D. J., Evitt, E. R.; Loffler, D. G.; Wentrcek, P. R., Voss, V.; Masuda, T., A mercury-catalyzed, high-yield system for the oxidation of methane to methanol. *Science* **1993**, 259, 340-343.

(6) Periana, R. A.; Taube, D. J.; Gamble, S.; Taube, H.; Satoh, T.; Fujii, H., Platinum catalysts for the high-yield oxidation of methane to a methanol derivative. *Science* **1998**, 280 (5363), 560-564.

(7) Cui, X.; Li, H.; Wang, Y.; Hu, Y.; Hua, L.; Li, H.; Han, X.; Liu, Q.; Yang, F.; He, L.; Chen, X.; Li, Q.; Xiao, J.; Deng, D.; Bao, X., Room-Temperature Methane Conversion by Graphene-Confined Single Iron Atoms, *Chem*, **2018**, 4 ,1902-1910.

(8) Huang, W.; Zhang, S.; Tang, Y.; Li, Y.; Nguyen, L.; Li, Y.; Shan, J.; Xiao, D.; Gagne, R.; Frenkel, A.I.; Tao, F.F., Low-Temperature Transformation of Methane to Methanol on Pd_1O_4 Single Sites Anchored on the Internal Surface of Microporous Silicate, *Angew. Chem. Int. Ed.* **2016**, 55, 13441-13445.

(9) Zuo, Z.; Ramirez, P.J.; Senanayake, S.D.; Liu, P.; Rodriguez, J.A., Low-Temperature Conversion of Methane to Methanol on CeO_x/Cu_2O Catalysts: Water Controlled Activation of the C-H Bond, *J. Am. Chem. Soc.* **2016**, 138, 13810-13813.

(10) Liu, Z.; Huang, E.; Orozco, I.; Liao, W.; Palomino, R. M.; Rui, N.; Duchon, T.; Nemšák, S.; Grinter, D. C.; Mahapatra, M.; Liu, P.; Rodriguez, J. A.; Senanayake, S. D., Water-promoted interfacial pathways in methane oxidation to methanol on a CeO_2-Cu_2O catalyst, *Science*, **2020**, 368, 513-517.

(11) Tomkins, P.; Ranocchiari, M.; van Bokhoven, J. A., Direct conversion of methane to methanol under mild conditions over Cu-Zeolites and beyond. *Acc. Chem. Res.* **2017**, 50, 418-425.

(12) Dinh, K.T.; Sullivan, M.M.; Narsimhan, K.; Serna, P.; Meyer, R.J.; Dinca, M.; Roman-Leshkov, Y., Continuous Partial Oxidation of Methane to Methanol Catalyzed by Diffusion-Paired Copper Dimers in Copper-Exchanged Zeolites, *J. Am. Chem. Soc.* **2019**, 141, 11641-11650.

(13) Snyder, B. E.; Vanelderen, P.; Bols, M. L.; Hallaert, S. D.; Bottger, L. H.; Ungur, L.; Pierloot, K.; Schoonheydt, R. A.; Sels, B. F.; Solomon, E. I., The active site of low-temperature methane hydroxylation in iron-containing zeolites. *Nature* **2016**, 536, 317-321.

(14) Agarwal, N.; Freakley, S. J.; McVicker, R. U.; Althahban, S. M.; Dimitratos, N.; He, Q.; Morgan, D. J.; Jenkins, R. L.; Willock, D. J.; Taylor, S. H.; Kiely, C. J.; Hutchings, G. J., Aqueous Au-Pd colloids catalyze selective CH4 oxidation to CH_3OH with O_2 under mild conditions. *Science* **2017**, 358, 223–227.

(15) Ab Rahim, M. H.; Forde, M. M.; Jenkins, R. L.; Hammond, C.; He, Q.; Dimitratos, N.; Lopez-Sanchez, J. A.; Carley, A. F.; Taylor, S. H.; Willock, D. J.; Murphy, D. M.; Kiely, C. J.; Hutchings, G. J., Oxidation of methane to methanol with hydrogen peroxide using supported Gold–Palladium alloy nanoparticles. *Angew. Chem. Int. Ed.* **2013**, 52, 1280 –1284.

(16) Jin, Z.; Wang, L.; Zuidema, E.; Mondal, K.; Zhang, M.; Zhang, J.; Wang, C.; Meng, X.; Yang, H.; Mesters, C.; Xiao, F.; H_2O_2 Hydrophobic zeolite modification for in situ peroxide formation in methane oxidation to methanol, *Science*, **2020**, 367, 193–197.

(17) Sushkevich, V. L.; Palagin, D.; Ranocchiari, M.; van Bokhoven J. A., Selective anaerobic oxidation of methane enables direct synthesis of methanol. *Science* **2017**, 356, 523–527.

(18) Lee, S. H.; Kang, J. K.; Park, E. D., Continuous methanol synthesis directly from methane and steam over Cu(II)-exchanged mordenite. *Korean J. Chem. Eng.* **2018**, 35, 2145-2149.

(19) Koishybay, A.; Shantz, D. F., Water is the oxygen source for methanol produced in partial oxidation of methane in a flow reactor over Cu-SSZ-13. *J. Am. Chem. Soc.* **2020**, 142, 11962-11966.

(20) Periana, R. A. Comment on "Selective anaerobic oxidation of methane enables direct synthesis of methanol". *Science* **2017**, 358, eaan5970.

(21) Sushkevich, V. L.; Palagin, D.; Ranocchiari, M.; van Bokhoven, J. A., Response to Comment on "Selective anaerobic oxidation of methane enables direct synthesis of methanol". *Science* **2017**, 358, eaan6083.

(22) Sun, L.; Wang, Y.; Wang, C.; Xie, Z.; Guan, N.; Li L., Water-involved methane-selective catalytic oxidation by dioxygen over copper zeolites. *Chem* **2021**, 7, 1557-1568.

(23) Bogaerts, A.; Tu, X.; Whitehead, J. C.; Centi, G.; Lefferts, L.; Guaitella, O.; Azzolina-Jury, F.; Kim, H.-H.; Murphy, A. B.; Schneider, W. F.; Nozaki, T.; Hicks, J. C.; Rousseau, A.; Thevenet, F.; Khacef, A.; Carreon, M., The 2020 plasma catalysis roadmap. *J. Phys. D: Appl. Phys.* **2020**, 53, 443001.

(24) Cui, Z.; Meng, S.; Yi, Y.; Jafarzadeh, A.; Li, S.; Neyts, E.C.; Hao, Y.; Li, L.; Zhang, X.; Wang, X.; Bogaerts, A., Plasma-Catalytic Methanol Synthesis from CO_2 Hydrogenation over a Supported Cu Cluster Catalyst: Insights into the Reaction Mechanism, *ACS Catal.* **2022**, 1326-1337.

(25) Yi, Y.; Wang, X.; Jafarzadeh, A.; Wang, L.; Liu, P.; He, B.; Yan, J.; Zhang, R.; Zhang, H.; Liu, X.; Guo, H.; Neyts, E.C.; Bogaerts, A., Plasma-catalytic ammonia reforming of methane over Cu-based catalysts for the production of HCN and H_2 at reduced temperature, *ACS Catal.* **2021**, 11, 1765–1773.

(26) Chen, Q.; Meng, S.; Liu, R.; Zhai, X.; Wang, X.; Wang, L.; Guo, H.; Yi, Y., Plasma-catalytic CO_2 hydrogenation to methanol over CuO-MgO/Beta catalyst with high selectivity, *Appl.*

Catal. B: Environ. **2024**, 342, 123422.

(27) Okazaki, K.; Kishida, T.; Ogawa, K.; Nozaki, T., Direct conversion from methane to methanol for high efficiency energy system with exergy regeneration. *Energy Conv. Manag.* **2002**, 43, 1459–1468.

(28) Liu, J.-L.; Snoeckx, R.; Cha, M. S., Steam reforming of methane in a temperature-controlled dielectric barrier discharge reactor: the role of electron-induced chemistry versus thermochemistry. *J. Phys. D: Appl. Phys.* **2018**, 51, 385201.

(29) Tang, Y.; Cui, Y.; Ren, G.; Ma, K.; Ma, X.; Dai, C.; Song, C., One-step synthesis methanol and hydrogen of methanol and hydrogen from methane and water using non-thermal plasma and Cu-Mordenite catalyst. *Fuel Process. Technol.* **2023**, 224, 107722 (2023).

(30) Fang, W.; Wang, X.; Li, S.; Hao, Y.; Yang, Y.; Zhao, W.; Liu, R.; Li, D.; Li, C.; Gao, X.; Wang, L.; Guo, H.; Yi, Y., Oligomerized [Cu–O–Cu] species are reported to be efficient in promoting plasma catalytic one-step steam reforming of methane to methanol and hydrogen. *Green Chem.* **2024**, 26, 5150-5154.

(31) Kim, M., Lee, C., & Ha, B. TPR study on differently prepared copper mordenites. *Korean J. Chem. Eng.* **1992**, 9, 53-59.

(32) Torre-Abreu, C.; Rieiro, M. F.; Henriques, C.; Delahay, G., NO TPD and H_2-TPR studies for characterisation of CuMOR catalysts The role of Si/Al ratio, copper content and cocation. *Appl. Catal. B: Environ.* **1997**, 14, 261-272.

(33) Grundner, S.; Markovits, M. A.; Li, G.; Tromp, M.; Pidko, E. A.; Hensen, E. J.; Jentys, A.; Sanchez-Sanchez, M.; Lercher, J. A., Single-site trinuclear copper oxygen clusters in mordenite for selective conversion of methane to methanol. *Nat. Comm.* **2015**, 6, 7546.

(34) Groothaert, M.; Smeets, P.; Sels, B.; Jacobs, P.; Schoonheydt, R., Selective oxidation of methane by the Bis(μ-oxo)dicopper core stabilized on ZSM-5 and mordenite zeolites. *J. Am. Chem. Soc.* **2005**, 127, 1394-1395.

(35) Mahyuddin, M. H.; Tanaka, T.; Shiota, Y.; Staykov, A.; Yoshi-zawa, K., Methane Partial oxidation over $[Cu_2(\mu\text{-}O)]^{2+}$ and $[Cu_3(\mu\text{-}O)_3]^{2+}$ active species in large-pore Zeolites. *ACS Catal.* **2018**, 8, 1500-1509.

(36) Sushkevich, V. L.; Palagin, D.; van Bokhoven, J. A., The effect of the active-site structure on the activity of copper mordenite in the aerobic and anaerobic conversion of methane into methanol. *Angew. Chem. Int. Ed.* **2018**, 57, 8906-8910.

(37) S. Wang, W. Guo, L. Zhu, H. Wang, K. Qiu, K. Cen, Methyl acetate synthesis from dimethyl ether carbonylation over mordenite modified by cation exchange. *J. Phys. Chem. C* **2014**, 119, 524-533.

(38) Yi, Y.; Li, S.; Cui, Z.; Hao, Y.; Zhang, Y.; Wang, L.; Liu, P.; Tu, X.; Xu, X.; Guo, H.; Bogaerts, A., Selective oxidation of CH_4 to CH_3OH through plasma catalysis: Insights from catalyst characterization and chemical kinetics modelling. *Appl. Catal. B: Environ.* **2021**, 296, 120384.

(39) Martín, A. J.; Mitchell, S.; Mondelli, C.; Jaydev, S.; Pérez-Ramírez, J., Unifying views on catalyst deactivation. *Nat. Catal.* **2022**, 5, 854-866.

(40) Espinos, J. P.; Morales, J.; Barranco, A.; Caballero, A.; Holgado, J. P.; Gonzalez-Elipe a. r., Interface Effects for Cu, CuO, and Cu_2O Deposited on SiO_2 and ZrO_2. XPS determination of the valence state of copper in Cu/SiO_2 and Cu/ZrO_2 Catalysts. *J. Phys. Chem. B* **2002**, 106, 6921-6929.

(41) Artiglia, L.; Sushkevich, V. L.; Palagin, D.; Knorpp, A. J.; Roy, K.; van Bokhoven, J. A., In situ X-ray photoelectron spectroscopy detects multiple active sites involved in the selective anaerobic oxidation of methane in copper-exchanged zeolites. *ACS Catal.* **2019**, 9, 6728-6737.

(42) Groothaert, M. H.; van Bokhoven, J. A.; Battiston, A. A.; Weckhuysen, B. M.; Schoonheydt, R. A., Bis(μ-oxo)dicopper in Cu-ZSM-5 and its role in the decomposition of NO: A combined in situ XAFS, UV-Vis-Near-IR, and Kinetic Study. *J. Am. Chem. Soc.* **2003**, 125, 7629-7640.

(43) Kim, Y.; Kim, T. Y.; Lee, H.; Yi, J., Distinct activation of Cu-MOR for direct oxidation of methane to methanol. *Chem. Comm.* **2017**, 53, 4116-4119.

(44) Giordanino, F.; Vennestrøm, P. N. R.; Lundegaard, L. F.; Stappen, F. N.; Mossin, S.; Beato, P.; Bordiga, S.; Lamberti, C., Characterization of Cu-exchanged SSZ-13: a comparative FTIR, UV-Vis, and EPR study with Cu-ZSM-5 and Cu-beta with similar Si/Al and Cu/Al ratios. *Dalton Trans* **2013**, 42, 12741-12761.

(45) Wang, L.; Yi, Y.; Wu, C.; Guo, H.; Tu, X., One-Step reforming of CO_2 and CH_4 into high-value liquid chemicals and fuels at room temperature by plasma-driven catalysis. *Angew. Chem. Int. Ed.* **2017**, 56, 13679-13683.

(46) Li, S.; Sun, J.; Gorbanev, Y.; van't Veer, K.; Loenders, B.; Yi, Y.; Kenis, T.; Chen, Q.; Bogaerts, A., Plasma-Assisted Dry Reforming of CH_4: How Small Amounts of O_2 Addition Can Drastically Enhance the Oxygenate Production ─ Experiments and Insights from Plasma Chemical Kinetics Modeling, *ACS Sustainable Chem. Eng.* **2023**, 11, 15373-15384.

(47) Chawdhury, P.; Wang, Y.; Ray, D.; Mathieu, S.; Wang, N.; Harding, J.; Bin, F.; Tu, X.; Subrahmanyam, C., A promising plasma-catalytic approach towards single-step methane conversion to oxygenates at room temperature. *Appl. Catal. B: Environ.* **2021**, 284, 119735.

(48) De Bie, C., van Dijk, J.; Bogaerts, A. The dominant pathways for the conversion of methane into oxygenates and syngas in an atmospheric pressure dielectric barrier discharge. *J. Phys. Chem. C* **2015**, 119, 22331-22350.

(49) Snoeckx, R.; Ozkan, A.; Reniers, F.; Bogaerts A. The quest for value-added products from carbon dioxide and water in a dielectric barrier discharge plasma: a chemical kinetics study, *ChemSusChem* **2017**, 10, 409-424.

Supporting Information

Plasma-catalytic One-step Steam Reforming of Methane to Methanol: Revealing the Catalytic Cycle on Cu/MOR

Yingzi Hao,[1, #] Shangkun Li,[2 #] Wei Fang,[1] Ximiao Wang,[1] Zhaolun Cui,[3] Kristof M. Bal,[2] Nick Gerrits,[2] Hongchen Guo,[1] Erik C. Neyts,[2] Annemie Bogaerts,[2] Yanhui Yi [1]*

[1]State Key Laboratory of Fine Chemicals, Frontier Science Center for Smart Materials, School of Chemical Engineering, Dalian University of Technology, Dalian 116024, P.R. China.

[2]Research group PLASMANT, Department of Chemistry, University of Antwerp, Universiteitsplein 1, BE-2610 Wilrijk-Antwerp, Belgium.

[3]School of Electric Power Engineering, South China University of Technology, Guangzhou 510630, China.

Table of Contents

S1. Calculation of conversion, product selectivity and energy efficiency

To evaluate the reaction performance of the catalyst, the conversion of the reactants and the selectivity of the main products were calculated by the following equations. All product concentrations were obtained by standard curves.

The CH_4 conversion was calculated by:

$$X_{CH_4}(\%) = \frac{n_{CH_4}^{inlet} - n_{CH_4}^{outlet}}{n_{CH_4}^{inlet}} \times 100\% \quad (S1)$$

Where X represents the gas conversion, n represents the moles of reactants or products.

The selectivity of the gaseous products was calculated as：

$$S_{C_2H_6}(\%) = \frac{2n_{C_2H_6}^{outlet}}{n_{CH_4}^{inlet} - n_{CH_4}^{outlet}} \times 100\% \quad (S2)$$

$$S_{C_2H_4}(\%) = \frac{2n_{C_2H_4}^{outlet}}{n_{CH_4}^{inlet} - n_{CH_4}^{outlet}} \times 100\% \quad (S3)$$

$$S_{C_3H_6}(\%) = \frac{3n_{C_3H_6}^{outlet}}{n_{CH_4}^{inlet} - n_{CH_4}^{outlet}} \times 100\% \quad (S4)$$

$$S_{CO}(\%) = \frac{n_{CO}^{outlet}}{n_{CH_4}^{inlet} - n_{CH_4}^{outlet}} \times 100\% \quad (S5)$$

$$Sco_2(\%) = \frac{n_{co_2}^{outlet}}{n_{CH_4}^{inlet} - n_{CH_4}^{outlet}} \times 100\% \quad (S6)$$

The selectivity of the liquid products was calculated as follows:

$$\text{Total selectivity of liquid product}(\%) = 100\% - (S_{C_2H_6} + S_{C_2H_4} + S_{C_3H_6} + S_{CO} + Sco_2) \quad (S7)$$

$$S_{C_xH_yO_Z}(\%) = \frac{xn_{C_xH_yO_Z}}{n_{CH_3OH} + 2n_{C_2H_5OH} + 2n_{CH_3CHO} + 2n_{CH_3COOH}} \times \text{Total selectivity of liquid product}(\%) \quad (S8)$$

Where $n_{C_xH_yO_z}$ represents the number of moles of various oxygenates in the liquid fraction. Note that equation (S9) is only valid when the amount of coking is negligible, which is the case in our experiments. Additionally, we estimate the H_2O conversion (S10) based on the oxygen balance, and then we calculate the H_2 selectivity (S11).

$$X_{H_2O}(\%) = \frac{n_{CO}^{outlet} + 2n_{CO_2}^{outlet} + z \times n_{n\,C_xH_yO_z}^{outlet}}{n_{H_2O}^{inlet}} \times 100\% \quad (S9)$$

$$S_{H_2}(\%) = \frac{n_{H_2}^{outlet}}{2 \times n_{CH_4}^{inlet} \times X_{CH_4} + n_{H_2O}^{inlet} \times X_{H_2O}} \times 100\% \quad (S10)$$

The energy consumption for the production of CH_3OH was defined as follows:

$$\text{Energy consumption (kJ/mmol)} = \frac{\text{discharge power (kJ/s)}}{\text{rate of } CH_3OH \text{ produced (mmol/s)}} \quad (S11)$$

Table S1. Standard curve formula of all substances in the system

Products	Equation	Adj. R-Square
CH_4	$Y=3.96820507*10^6*X + 65036.71$	0.999
C_2H_6	$Y =7.4515*10^6*X$	0.999
C_2H_4	$Y =7.55518*10^6*X$	0.999
C_3H_6	$Y =1.6011374*10^7*X$	0.998
CO	$Y =1.04671*10^7* X$	0.998
CH_3OH	$Y=9.27044*10^4*X$	0.998
C_2H_5OH	$Y=1.18790*10^5*X$	0.999
CH_3CHO	$Y=2.96785*10^4*X$	0.998
CH_3COOH	$Y=4.96131*10^4*X$	0.999

X represents the concentration of liquid sample (mol/L); Y represents the peak area of the sample.

S2. Liquid products: Qualitative analysis

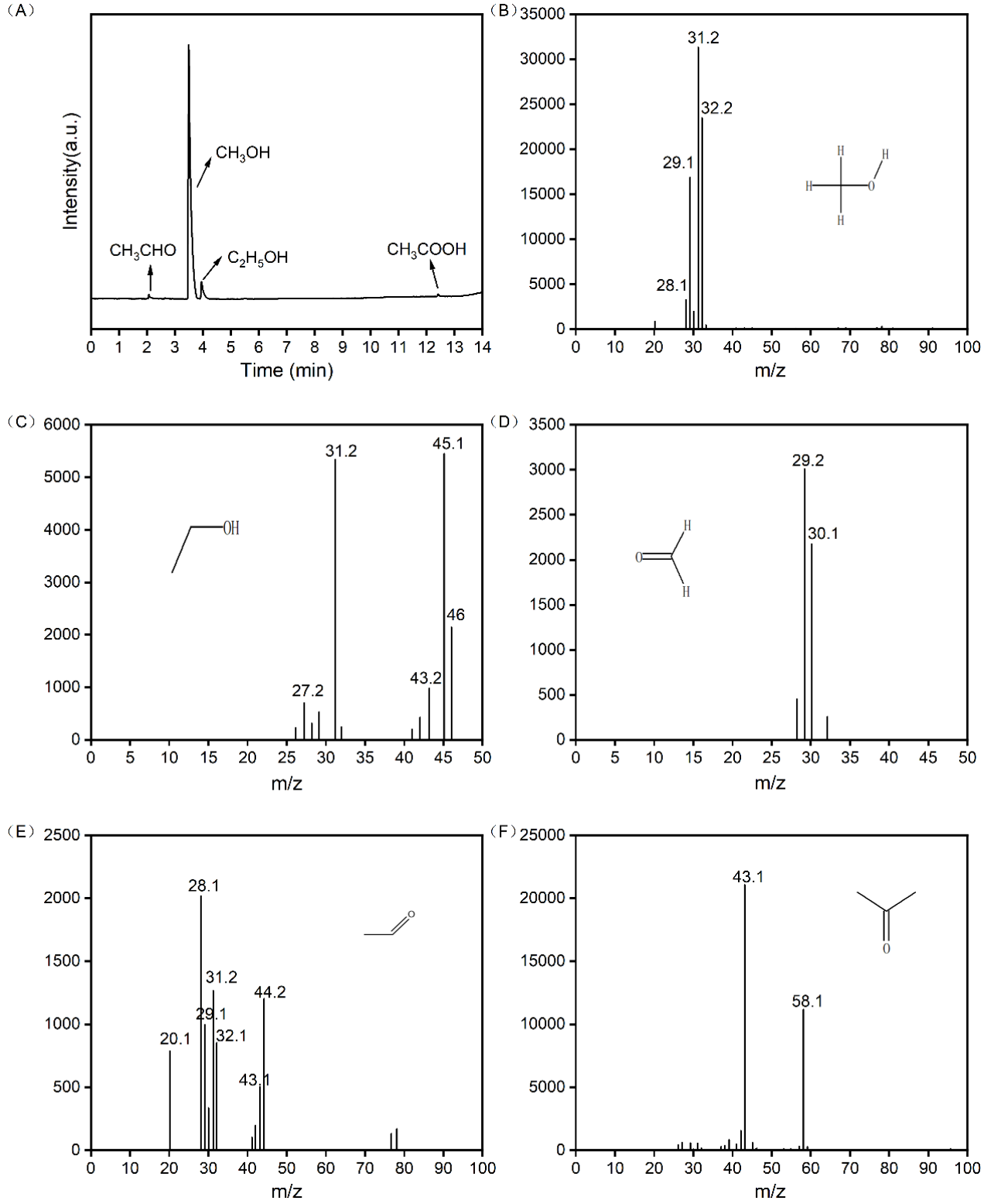

Figure S1. Results of qualitative analysis of liquid products. (A) Gas chromatography, indicating the presence of CH_3OH, C_2H_5OH, CH_3CHO and CH_3COOH. GC-MS analysis results. (B) Methanol; (C) Ethanol; (D) Formaldehyde; (E) Acetaldehyde; (F) Acetone. Note that acetone is the wash solution, resulting in higher acetone abundance in the GC-MS results than the actual amount produced.

The liquid products were qualitatively analyzed by gas chromatography (GC) and gas chromatography mass spectrometry (GC-MS), as shown in Figure S1. GC results (Figure S1A) show the presence of CH_3OH, C_2H_5OH, CH_3CHO and CH_3COOH. We used the external standard method to quantify the liquid products. In addition, the MS signals of methanol, ethanol, formaldehyde, and acetaldehyde are listed in Figure S1B – S1E. Note that acetone (S1F) is the wash solution, resulting in higher acetone abundance in the GC-MS results. In summary, the liquid products mainly include CH_3OH, HCHO, C_2H_5OH, CH_3CHO and CH_3COOH by qualitative analysis of GC and GC-MS.

S3. Optimization of reaction conditions

The temperature (Figure S2A) and CH_4/H_2O ratio (Figure S2B) have been tested with Cu/MOR catalyst on plasma-catalytic OSRMtM. The CH_4 conversion increased with temperature from 130 ºC to 290 ºC, but the CH_3OH selectivity reached a peak at 170 ºC. In order to maximize the CH_3OH production, we continued our experiments at 170 ºC. By investigating different CH_4/H_2O ratios, an optimal CH_4/H_2O ratio was 1:4, with 77 % CH_3OH selectivity was found. Therefore, we study the plasma-catalytic OSRMtM reaction performance and the mechanisms under the optimized reaction conditions (170 ºC; CH_4/H_2O ratio = 1:4).

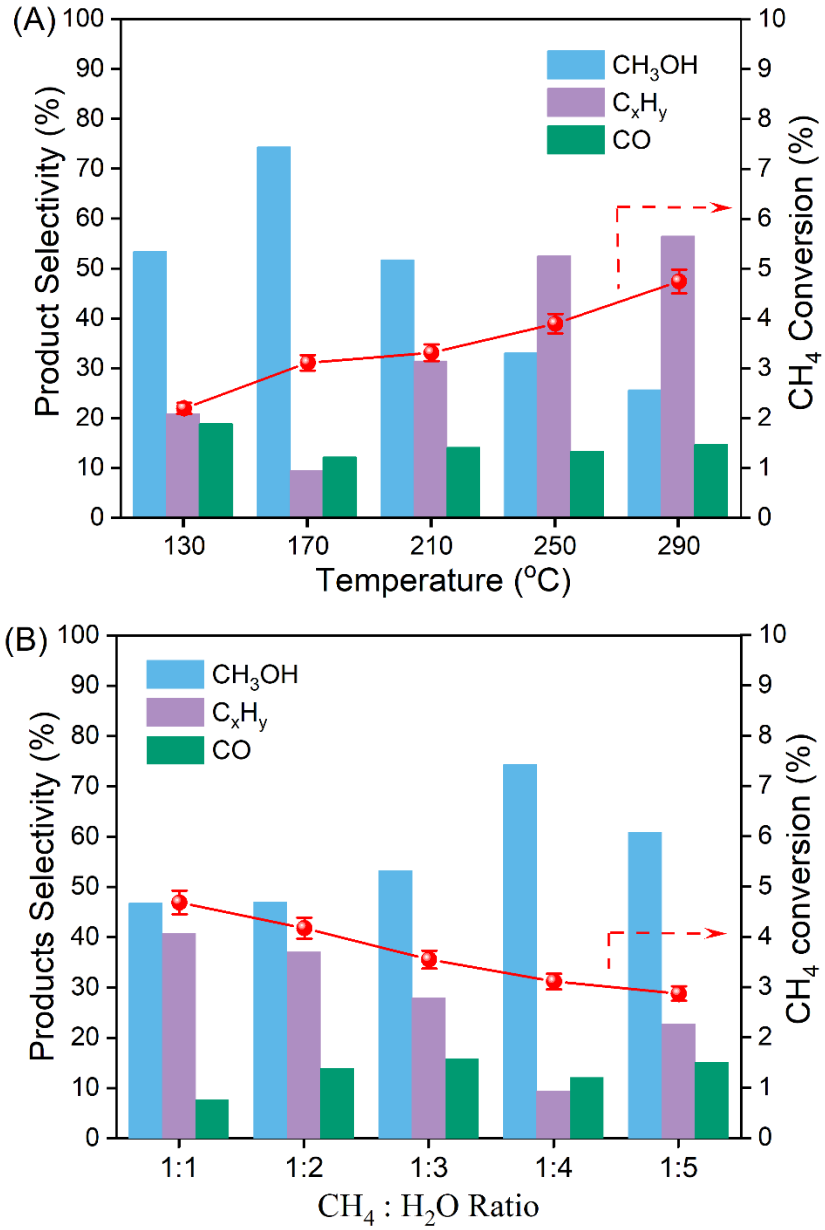

Figure S2. Experimental results of OSRMtM with Cu/MOR, varying (A) temperature and (B) the ratio of CH_4 and H_2O. Reaction conditions: 1.7 wt.% Cu loading; discharge length: 5 cm; discharge power: 7 W; total flow rate: 100 ml/min.

S4. Energy consumption at different conditions

The discharge voltage and current were measured by a digital fluorescence oscilloscope (Tektronix, DPO 3012) with a high voltage probe (Tektronix P6015) and a current probe (Pearson 6585) to obtain the Lissajous figures, which were used to calculate the plasma power and monitor the discharge properties. As shown in Figure S3, packing Cu/MOR catalyst can slightly reduce the discharge power compared to MOR catalyst. The energy consumption for CH_3OH production through plasma-catalytic OSRMtM by the Cu/MOR catalyst is (only) 22.7 kJ/mmol (Figure S3), which is much lower than with plasma only (79.7 kJ/mmol) and plasma + MOR (114.3 kJ/mmol).

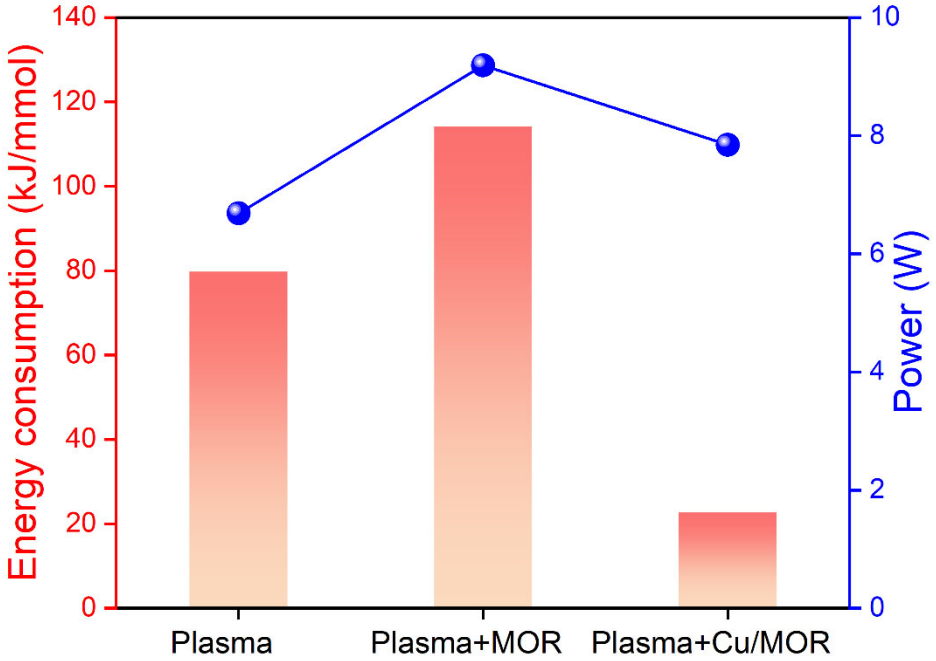

Figure S3. Energy consumption for CH_3OH production, and discharge power, for plasma only, plasma + MOR, and plasma + Cu/MOR at 443 K.

S5. Comparison of this work with literature results with H_2O as oxidant

Table S2. Summary of plasma catalysis and thermal catalysis for OSRMtM performance.

Plasma catalysis in this paper			
Catalyst	**Conditions**	**CH_4 conversion (%)**	**CH_3OH selectivity (%)**
MOR	170 °C; 1 bar	2.0	26.7
Cu-MOR IE1		2.4	51.8
Cu/MOR IE2		3.0	70.9
Cu/MOR IE3		2.9	70.7
Cu/MOR IE4		3.0	77.0
Cu/MOR IE5		3.0	71.5

Thermal catalysis from literature				
Catalyst	**Conditions**	**CH_4 conversion (%)**	**CH_3OH selectivity (%)**	**CH_3OH yield ($mmol/mol_{Cu}$ /h)**
Cu-H-MOR [1]	350 °C	0.001335	100%	20.8±2.6
Cu-SSZ-13 [2]	225 °C	0.000187	~	12.7±0.4
Cu-CHA [3]	300°C	0.0136	91%	543
Cu-MOR [4]	350 °C	~	~	33
Cu/MOR [5]	200 °C	0.106	97%	0.41
Cu/MOR [6]	200 °C	0.072	98%	0.37

Plasma and plasma catalysis from literature			
Catalyst	**Conditions**	**CH_4 conversion (%)**	**CH_3OH selectivity (%)**
Plasma only [7]	CH_4: H_2O=1:1; 3 W	5	20
Plasma only [8]	CH_4: H_2O=1:5; 120°C	1.07	7.5
Plasma + TiO_2 [9]	35 °C; 1 bar; 30 W	~	93 (only in liquid phase)
Plasma + Cu/MOR [10]	120 °C; 1 bar; 30 W	~ 3	< 30 (86 only in the liquid phase)

In order to estimate the difference in performance between plasma catalysis and thermal catalysis, we calculate the CH_4 conversion based on the corresponding reference results by equation (S12). The CH_4 flow rate was converted to standard conditions (25 °C, 1 bar). As shown in Table S2, the difference in the reaction conditions result in the orders of magnitude differences in CH_4 conversion in thermal catalysis mainly due to the multi-step catalytic cycle reactions, i.e., a non-continuous process.

$$X_{CH_4}(\%) = \frac{Y_{CH3OH}/S_{CH3OH}}{n_{CH4}} \times 100\% \qquad \text{(S12)}$$

S6. Physicochemical properties of Cu/MOR catalysts

Table S3. Physicochemical properties of Cu/MOR catalysts.

Catalyst	Si/Al ratio	Cu/Al ratio	Cu loading (wt.%)	S_{BET} (m^2g^{-1})	V_{micro} (cm^3g^{-1})	Pore Size （nm）
MOR	17.0	0.000	0.000	596.0	0.216	1.668
Cu/MOR IE-1	17.8	0.10	0.94	543.4	0.195	1.700
Cu/MOR IE-2	18.2	0.15	1.34	521.1	0..187	1.690
Cu/MOR IE-3	18.5	0.16	1.52	531.7	0.191	1.717
Cu/MOR IE-4	18.6	0.20	1.78	521.0	0.191	1.632
Cu/MOR IE-5	18.5	0.21	1.96	453.6	0.167	1.649

N_2-physisorption was performed at -196 °C on a Micromeritics ASAP 2020 instrument to obtain structural information. Prior to the measurements, the samples were degassed under vacuum at 400 °C for 6 hours. The surface area was calculated by the Brunauer, Emmett and Teller (BET) method and the pore volume was obtained by the t-plot method. As shown in Table S3 and Figure S4, there is no evident change on the surface area, average pore size and pore volume of the Cu/MOR catalysts with four times Cu exchange. However, the surface area significantly decreased after five times change, indicating larger Cu clusters agglomeration on the MOR support. According to the IUPAC classification, all isotherms in Figure S4 belong to type I curves, which are typical for microporous materials.

S7. Nitrogen adsorption-desorption isotherms

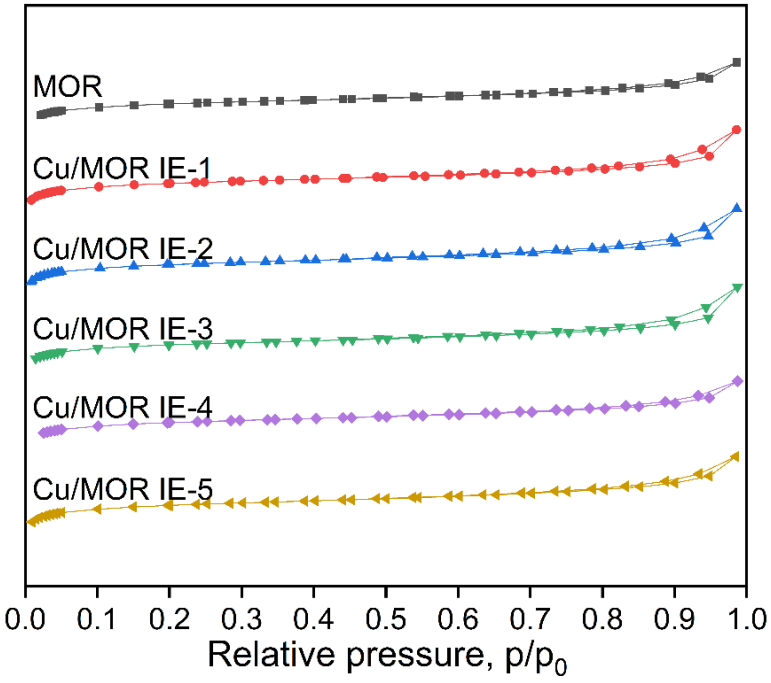

Figure S4. Nitrogen adsorption-desorption isotherms obtained at 77K for Cu/MOR samples.

S8. HRTEM

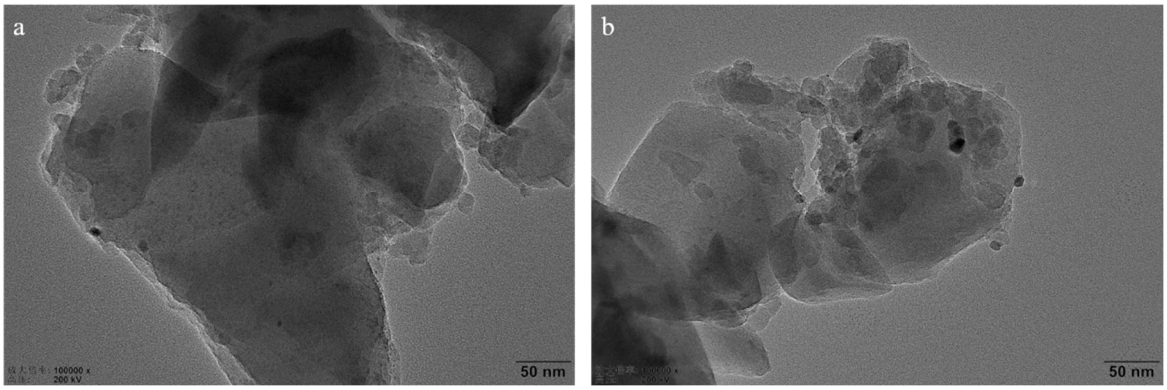

Figure S5. HRTEM patterns of (a) fresh Cu/MOR IE-4 catalyst and (b) spent Cu/MOR IE-4 catalyst.

High resolution transmission electron microscopy (HRTEM) was performed on JEM-2100F with an accelerating voltage of 200 kV. As shown in Figure S5, there are no evident copper particles on the Cu/MOR surface.

S9. NH_3-TPD

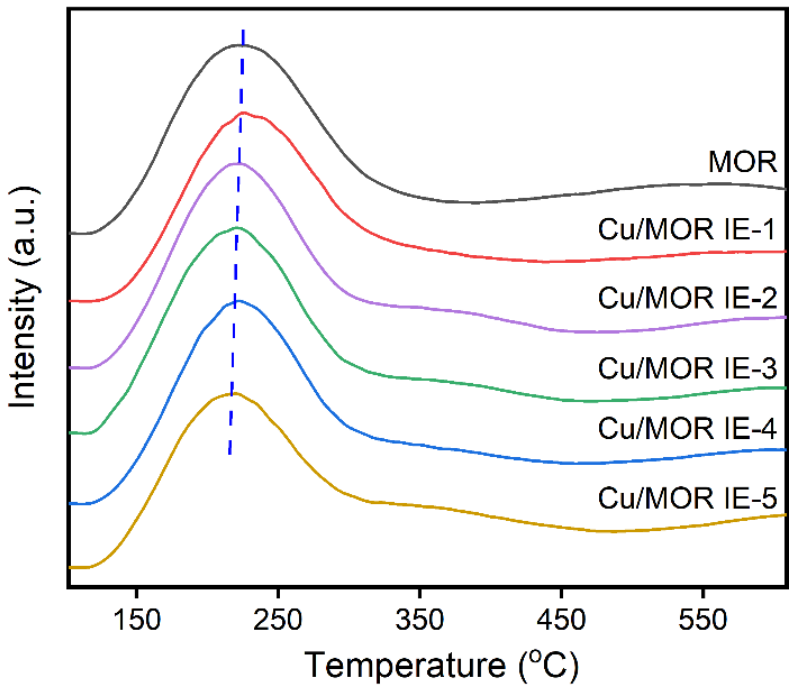

Figure S6. NH_3-TPD patterns of the fresh Cu/MOR catalysts with different exchange levels.

The acidity of the MOR and Cu-MOR samples was measured by NH_3 temperature programmed desorption (NH_3-TPD) and infrared spectroscopy of pyridine adsorption (Py-IR). The NH_3-TPD profile (Figure S6) shows simple MOR zeolites desorbing NH_3 in two different temperature ranges: a low temperature desorption range corresponding to weakly bound NH_3, and another high temperature range corresponding to relative strongly bound NH_3. The new desorption peak at around 320 °C after Cu ion exchange is attributed to NH_3 adsorption on sites of medium acidity, thus indicating the formation of new acidic sites, while strong acidic sites disappear and the central temperature of weak acidic sites shifts to lower temperatures, indicating weakening of the acidic strength.[11]

S10. Three experiments of Cu-MOR catalyst treated by different plasmas

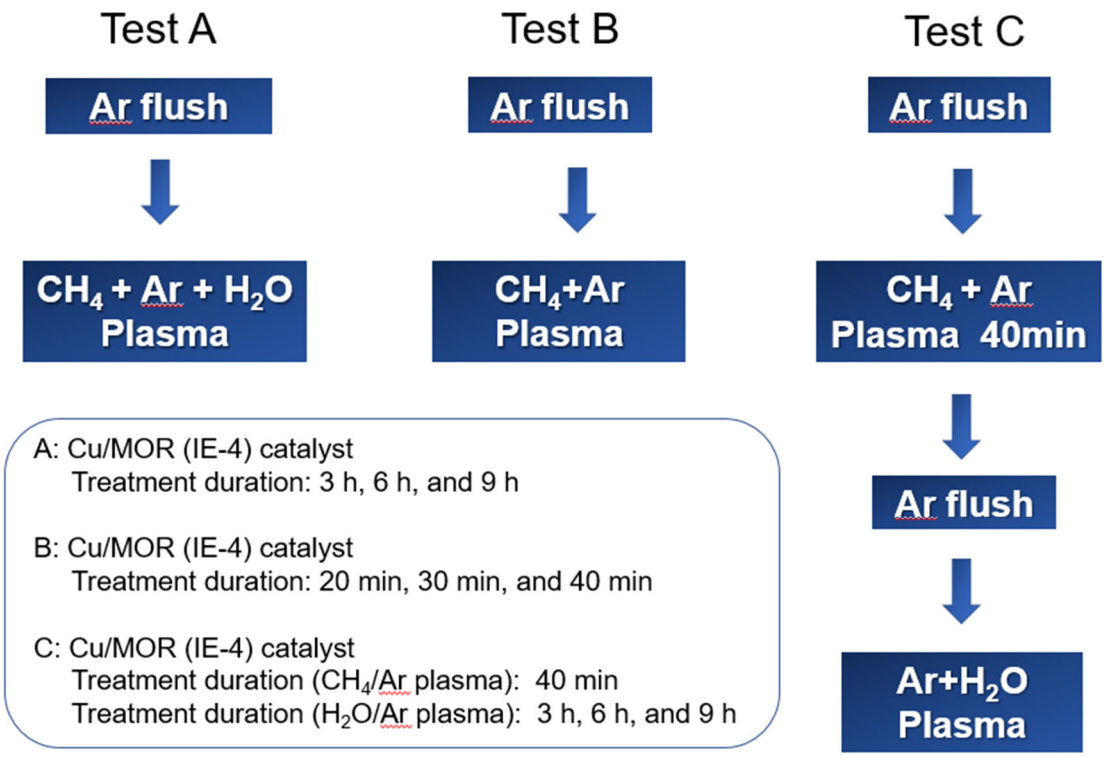

Figure S7. Diagram of Cu/MOR catalysts treated under different plasma conditions

S11. Lissajous plots under different conditions

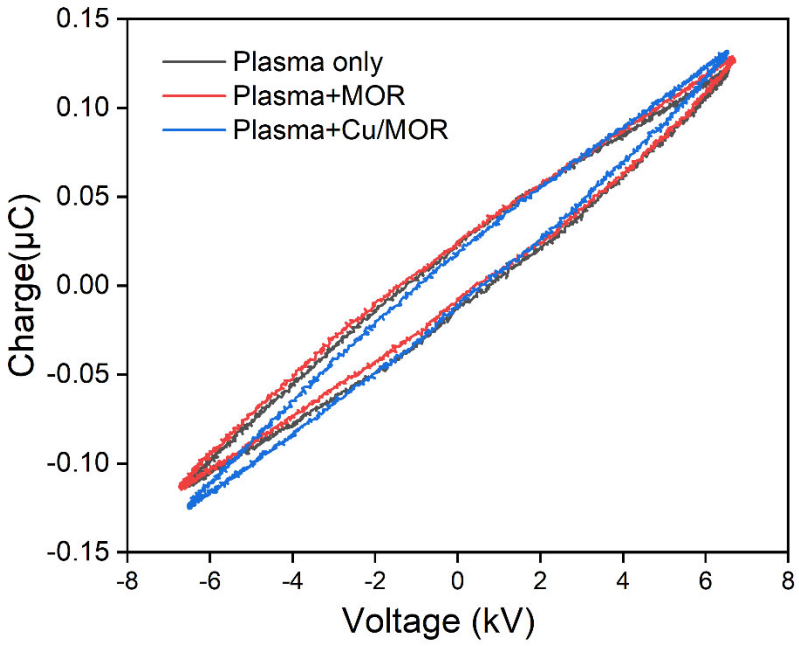

Figure S8. Lissajous plots for plasma only, plasma + MOR, and plasma + Cu/MOR at 443 K.

The Lissajous figures (Figure S8) of plasma, plasma + MOR and plasma + Cu/MOR were used to calculate the plasma power and monitor the discharge properties. There is no evident change in the Lissajous figures between plasma + MOR and plasma + Cu/MOR.

References

(1) Jeong, Y. R.; Jung, H.; Kang, J.; Han, J. W.; Park, E. D., Continuous synthesis of methanol from methane and steam over copper-mordenite. *ACS Catal.* **2021**, 11 (3), 1065-1070.

(2) Koishybay, A.; Shantz, D. F., Water is the oxygen source for methanol produced in partial oxidation of methane in a flow reactor over Cu-SSZ-13. *J. Am. Chem. Soc.* **2020**, 142, 11962-11966.

(3) Sun, L.; Wang, Y.; Wang, C.; Xie, Z.; Guan, N.; Li, L., Water-involved methane-selective catalytic oxidation by dioxygen over copper zeolites. *Chem* **2021**, 7, 1557-1568.

(4) Lee, S. H.; Kang, J. K.; Park, E. D., Continuous methanol synthesis directly from methane and steam over Cu(II)-exchanged mordenite. *Korean J. of Chem. Eng.* **2018**, 35, 2145-2149.

(5) Sushkevich, V. L.; Palagin, D.; Ranocchiari, M.; van Bokhoven, J. A., Selective anaerobic oxidation of methane enables direct synthesis of methanol. *Science* **2017**, 356, 523–527.

(6) Sushkevich, V. L.; Palagin, D.; van Bokhoven, J. A., The effect of the active-site structure on the activity of copper mordenite in the aerobic and anaerobic conversion of methane into methanol. *Angew. Chem. Int. Ed.* **2018**, 57, 8906-8910.

(7) Takayuki., T.; Iizuka, S., Conversion of methane to methanol by a low-pressure steam plasma. *J. Environ. Eng. Technol* **2013**, 2, 35-39.

(8) Okazaki, K.; Kishida, T.; Ogawa, K.; Nozaki, T., Direct conversion from methane to methanol for high efficiency energy system with exergy regeneration. *Energy Conv. Manag.* **2002**, 43, 1459–1468.

(9) Bi, W.; Tang, Y.; Li, X.; Dai, C.; Song, C.; Guo, X.; Ma, X., One-step direct conversion of methane to methanol with water in non-thermal plasma. *Commun. Chem.* **2022**, 5, 124.

(10) Tang, Y.; Cui, Y.; Ren, G.; Ma, K.; Ma, X.; Dai, C.; Song, C., One-step synthesis methanol and hydrogen of methanol and hydrogen from methane and water using non-thermal plasma and Cu-Mordenite catalyst. *Fuel Process. Technol.* **2023**, 224, 107722.

(11) Wang, S.; Guo, W.; Zhu, L.; Wang, H.; Qiu, K.; Cen, K., Methyl acetate synthesis from dimethyl ether carbonylation over mordenite modified by cation exchange. *J. Phys. Chem. C* **2014**, 119, 524-533.

Supporting Information

Plasma-catalytic One-step Steam Reforming of Methane to Methanol: Revealing the Catalytic Cycle on Cu/MOR

Yingzi Hao,[1, #] Shangkun Li,[2 #] Wei Fang,[1] Ximiao Wang,[1] Zhaolun Cui,[3] Kristof M. Bal,[2] Nick Gerrits,[2] Hongchen Guo,[1] Erik C. Neyts,[2] Annemie Bogaerts,[2] Yanhui Yi [1]*

[1]State Key Laboratory of Fine Chemicals, Frontier Science Center for Smart Materials, School of Chemical Engineering, Dalian University of Technology, Dalian 116024, P.R. China.

[2]Research group PLASMANT, Department of Chemistry, University of Antwerp, Universiteitsplein 1, BE-2610 Wilrijk-Antwerp, Belgium.

[3]School of Electric Power Engineering, South China University of Technology, Guangzhou 510630, China.

Table of Contents

S1. Calculation of conversion, product selectivity and energy efficiency

To evaluate the reaction performance of the catalyst, the conversion of the reactants and the selectivity of the main products were calculated by the following equations. All product concentrations were obtained by standard curves.

The CH_4 conversion was calculated by:

$$X_{CH_4}(\%) = \frac{n_{CH_4}^{inlet} - n_{CH_4}^{outlet}}{n_{CH_4}^{inlet}} \times 100\% \quad \text{(S1)}$$

Where X represents the gas conversion, n represents the moles of reactants or products.

The selectivity of the gaseous products was calculated as：

$$S_{C_2H_6}(\%) = \frac{2n_{C_2H_6}^{outlet}}{n_{CH_4}^{inlet} - n_{CH_4}^{outlet}} \times 100\% \quad \text{(S2)}$$

$$S_{C_2H_4}(\%) = \frac{2n_{C_2H_4}^{outlet}}{n_{CH_4}^{inlet} - n_{CH_4}^{outlet}} \times 100\% \quad \text{(S3)}$$

$$S_{C_3H_6}(\%) = \frac{3n_{C_3H_6}^{outlet}}{n_{CH_4}^{inlet} - n_{CH_4}^{outlet}} \times 100\% \quad \text{(S4)}$$

$$S_{CO}(\%) = \frac{n_{CO}^{outlet}}{n_{CH_4}^{inlet} - n_{CH_4}^{outlet}} \times 100\% \quad \text{(S5)}$$

$$Sco_2(\%) = \frac{n_{co_2}^{outlet}}{n_{CH_4}^{inlet} - n_{CH_4}^{outlet}} \times 100\% \quad \text{(S6)}$$

The selectivity of the liquid products was calculated as follows:

$$\text{Total selectivity of liquid product}(\%) = 100\% - (S_{C_2H_6} + S_{C_2H_4} + S_{C_3H_6} + S_{CO} + Sco_2) \quad \text{(S7)}$$

$$S_{C_xH_yO_Z}(\%) = \frac{xn_{C_xH_yO_Z}}{n_{CH_3OH} + 2n_{C_2H_5OH} + 2n_{CH_3CHO} + 2n_{CH_3COOH}} \times \text{Total selectivity of liquid product}(\%) \quad \text{(S8)}$$

Where $n_{C_xH_yO_z}$ represents the number of moles of various oxygenates in the liquid fraction. Note that equation (S9) is only valid when the amount of coking is negligible, which is the case in our experiments. Additionally, we estimate the H_2O conversion (S10) based on the oxygen balance, and then we calculate the H_2 selectivity (S11).

$$X_{H_2O}(\%) = \frac{n_{CO}^{outlet} + 2n_{CO_2}^{outlet} + z \times n_{n\,C_xH_yO_z}^{outlet}}{n_{H_2O}^{inlet}} \times 100\% \quad \text{(S9)}$$

$$S_{H_2}(\%) = \frac{n_{H_2}^{outlet}}{2 \times n_{CH_4}^{inlet} \times X_{CH_4} + n_{H_2O}^{inlet} \times X_{H_2O}} \times 100\% \quad \text{(S10)}$$

The energy consumption for the production of CH_3OH was defined as follows:

$$\text{Energy consumption (kJ/mmol)} = \frac{\text{discharge power (kJ/s)}}{\text{rate of } CH_3OH \text{ produced (mmol/s)}} \quad \text{(S11)}$$

Table S1. Standard curve formula of all substances in the system

Products	Equation	Adj. R-Square
CH_4	$Y=3.96820507*10^6*X + 65036.71$	0.999
C_2H_6	$Y =7.4515*10^6*X$	0.999
C_2H_4	$Y =7.55518*10^6*X$	0.999
C_3H_6	$Y =1.6011374*10^7*X$	0.998
CO	$Y =1.04671*10^7* X$	0.998
CH_3OH	$Y=9.27044*10^4*X$	0.998
C_2H_5OH	$Y=1.18790*10^5*X$	0.999
CH_3CHO	$Y=2.96785*10^4*X$	0.998
CH_3COOH	$Y=4.96131*10^4*X$	0.999

X represents the concentration of liquid sample (mol/L); Y represents the peak area of the sample.

S2. Liquid products: Qualitative analysis

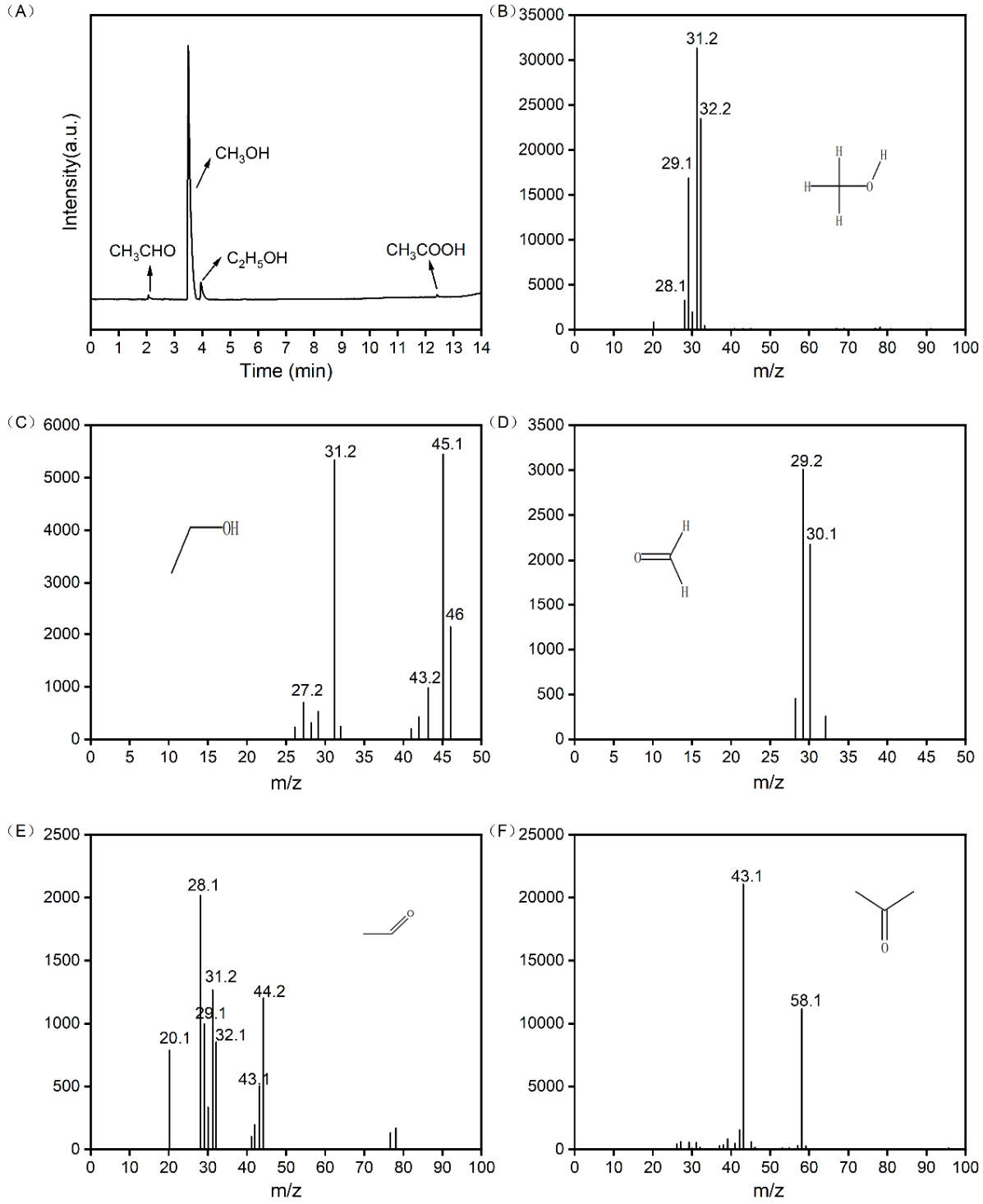

Figure S1. Results of qualitative analysis of liquid products. (A) Gas chromatography, indicating the presence of CH_3OH, C_2H_5OH, CH_3CHO and CH_3COOH. GC-MS analysis results. (B) Methanol; (C) Ethanol; (D) Formaldehyde; (E) Acetaldehyde; (F) Acetone. Note that acetone is the wash solution, resulting in higher acetone abundance in the GC-MS results than the actual amount produced.

The liquid products were qualitatively analyzed by gas chromatography (GC) and gas chromatography mass spectrometry (GC-MS), as shown in Figure S1. GC results (Figure S1A) show the presence of CH_3OH, C_2H_5OH, CH_3CHO and CH_3COOH. We used the external standard method to quantify the liquid products. In addition, the MS signals of methanol, ethanol, formaldehyde, and acetaldehyde are listed in Figure S1B – S1E. Note that acetone (S1F) is the wash solution, resulting in higher acetone abundance in the GC-MS results. In summary, the liquid products mainly include CH_3OH, HCHO, C_2H_5OH, CH_3CHO and CH_3COOH by qualitative analysis of GC and GC-MS.

S3. Optimization of reaction conditions

The temperature (Figure S2A) and CH_4/H_2O ratio (Figure S2B) have been tested with Cu/MOR catalyst on plasma-catalytic OSRMtM. The CH_4 conversion increased with temperature from 130 °C to 290 °C, but the CH_3OH selectivity reached a peak at 170 °C. In order to maximize the CH_3OH production, we continued our experiments at 170 °C. By investigating different CH_4/H_2O ratios, an optimal CH_4/H_2O ratio was 1:4, with 77 % CH_3OH selectivity was found. Therefore, we study the plasma-catalytic OSRMtM reaction performance and the mechanisms under the optimized reaction conditions (170 °C; CH_4/H_2O ratio = 1:4).

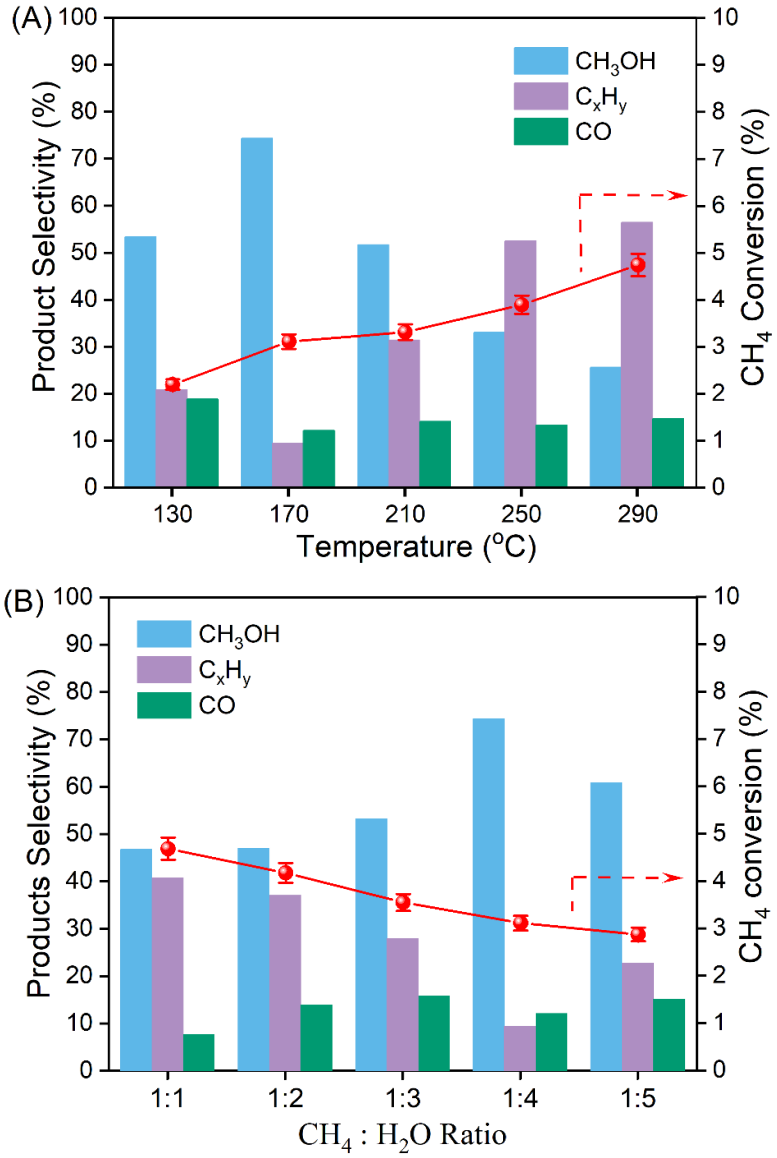

Figure S2. Experimental results of OSRMtM with Cu/MOR, varying (A) temperature and (B) the ratio of CH_4 and H_2O. Reaction conditions: 1.7 wt.% Cu loading; discharge length: 5 cm; discharge power: 7 W; total flow rate: 100 ml/min.

S4. Energy consumption at different conditions

The discharge voltage and current were measured by a digital fluorescence oscilloscope (Tektronix, DPO 3012) with a high voltage probe (Tektronix P6015) and a current probe (Pearson 6585) to obtain the Lissajous figures, which were used to calculate the plasma power and monitor the discharge properties. As shown in Figure S3, packing Cu/MOR catalyst can slightly reduce the discharge power compared to MOR catalyst. The energy consumption for CH_3OH production through plasma-catalytic OSRMtM by the Cu/MOR catalyst is (only) 22.7 kJ/mmol (Figure S3), which is much lower than with plasma only (79.7 kJ/mmol) and plasma + MOR (114.3 kJ/mmol).

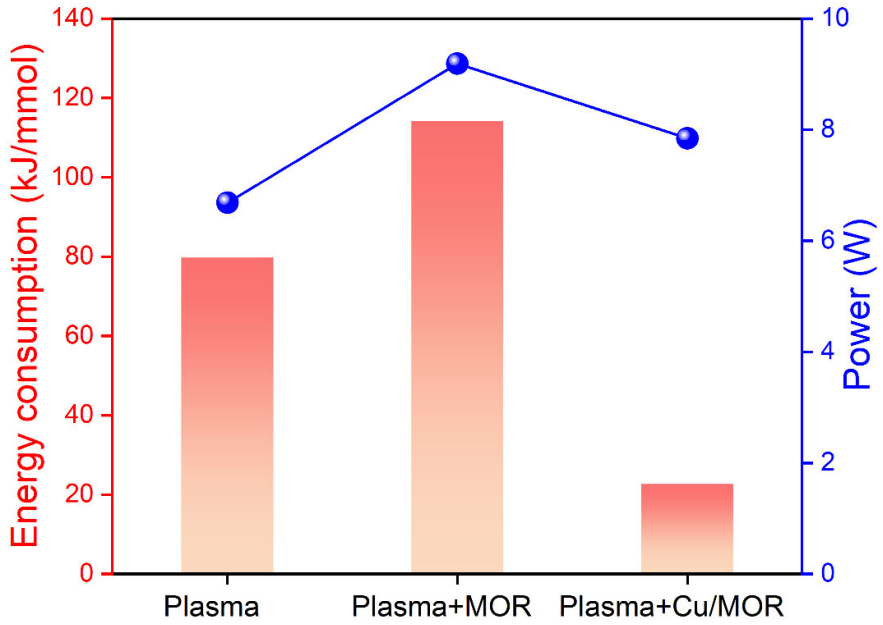

Figure S3. Energy consumption for CH_3OH production, and discharge power, for plasma only, plasma + MOR, and plasma + Cu/MOR at 443 K.

S5. Comparison of this work with literature results with H_2O as oxidant

Table S2. Summary of plasma catalysis and thermal catalysis for OSRMtM performance.

Plasma catalysis in this paper			
Catalyst	**Conditions**	**CH_4 conversion (%)**	**CH_3OH selectivity (%)**
MOR	170 °C; 1 bar	2.0	26.7
Cu-MOR IE1		2.4	51.8
Cu/MOR IE2		3.0	70.9
Cu/MOR IE3		2.9	70.7
Cu/MOR IE4		3.0	77.0
Cu/MOR IE5		3.0	71.5

Thermal catalysis from literature				
Catalyst	**Conditions**	**CH_4 conversion (%)**	**CH_3OH selectivity (%)**	**CH_3OH yield (mmol/mol_{Cu} /h)**
Cu-H-MOR [1]	350 °C	0.001335	100%	20.8±2.6
Cu-SSZ-13 [2]	225 °C	0.000187	~	12.7±0.4
Cu-CHA [3]	300°C	0.0136	91%	543
Cu-MOR [4]	350 °C	~	~	33
Cu/MOR [5]	200 °C	0.106	97%	0.41
Cu/MOR [6]	200 °C	0.072	98%	0.37

Plasma and plasma catalysis from literature			
Catalyst	**Conditions**	**CH_4 conversion (%)**	**CH_3OH selectivity (%)**
Plasma only [7]	CH_4: H_2O=1:1; 3 W	5	20
Plasma only [8]	CH_4: H_2O=1:5; 120°C	1.07	7.5
Plasma + TiO_2 [9]	35 °C; 1 bar; 30 W	~	93 (only in liquid phase)
Plasma + Cu/MOR [10]	120 °C; 1 bar; 30 W	~ 3	< 30 (86 only in the liquid phase)

In order to estimate the difference in performance between plasma catalysis and thermal catalysis, we calculate the CH_4 conversion based on the corresponding reference results by equation (S12). The CH_4 flow rate was converted to standard conditions (25 °C, 1 bar). As shown in Table S2, the difference in the reaction conditions result in the orders of magnitude differences in CH_4 conversion in thermal catalysis mainly due to the multi-step catalytic cycle reactions, i.e., a non-continuous process.

$$X_{CH_4}(\%) = \frac{Y_{CH3OH}/S_{CH3OH}}{n_{CH4}} \times 100\% \qquad \text{(S12)}$$

S6. Physicochemical properties of Cu/MOR catalysts

Table S3. Physicochemical properties of Cu/MOR catalysts.

Catalyst	Si/Al ratio	Cu/Al ratio	Cu loading (wt.%)	S_{BET} (m^2g^{-1})	V_{micro} (cm^3g^{-1})	Pore Size （nm）
MOR	17.0	0.000	0.000	596.0	0.216	1.668
Cu/MOR IE-1	17.8	0.10	0.94	543.4	0.195	1.700
Cu/MOR IE-2	18.2	0.15	1.34	521.1	0..187	1.690
Cu/MOR IE-3	18.5	0.16	1.52	531.7	0.191	1.717
Cu/MOR IE-4	18.6	0.20	1.78	521.0	0.191	1.632
Cu/MOR IE-5	18.5	0.21	1.96	453.6	0.167	1.649

N_2-physisorption was performed at -196 °C on a Micromeritics ASAP 2020 instrument to obtain structural information. Prior to the measurements, the samples were degassed under vacuum at 400 °C for 6 hours. The surface area was calculated by the Brunauer, Emmett and Teller (BET) method and the pore volume was obtained by the t-plot method. As shown in Table S3 and Figure S4, there is no evident change on the surface area, average pore size and pore volume of the Cu/MOR catalysts with four times Cu exchange. However, the surface area significantly decreased after five times change, indicating larger Cu clusters agglomeration on the MOR support. According to the IUPAC classification, all isotherms in Figure S4 belong to type I curves, which are typical for microporous materials.

S7. Nitrogen adsorption-desorption isotherms

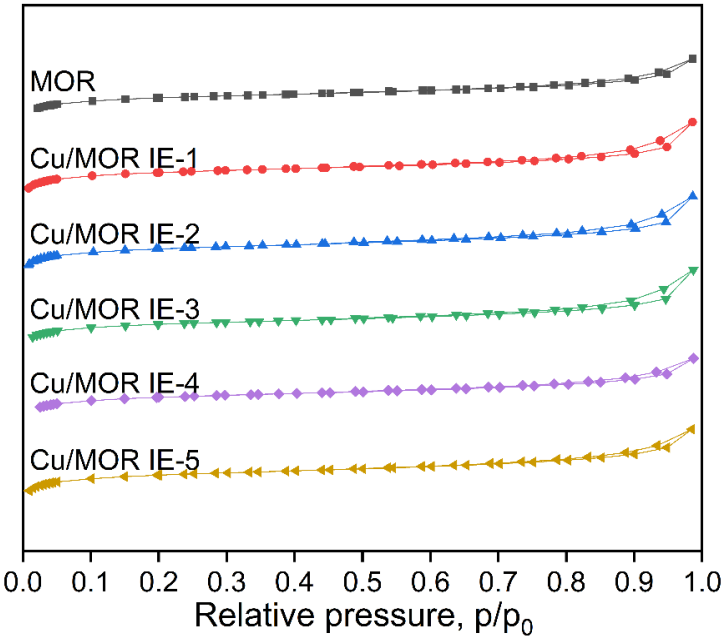

Figure S4. Nitrogen adsorption-desorption isotherms obtained at 77K for Cu/MOR samples.

S8. HRTEM

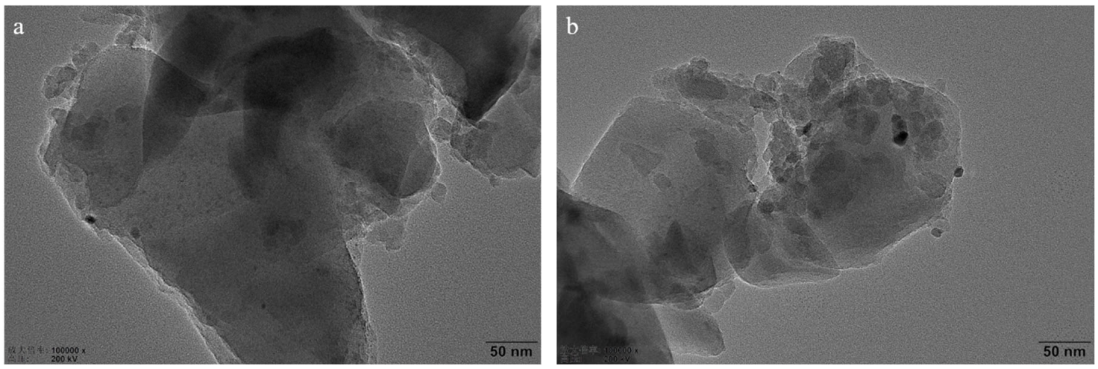

Figure S5. HRTEM patterns of (a) fresh Cu/MOR IE-4 catalyst and (b) spent Cu/MOR IE-4 catalyst.

High resolution transmission electron microscopy (HRTEM) was performed on JEM-2100F with an accelerating voltage of 200 kV. As shown in Figure S5, there are no evident copper particles on the Cu/MOR surface.

S9. NH_3-TPD

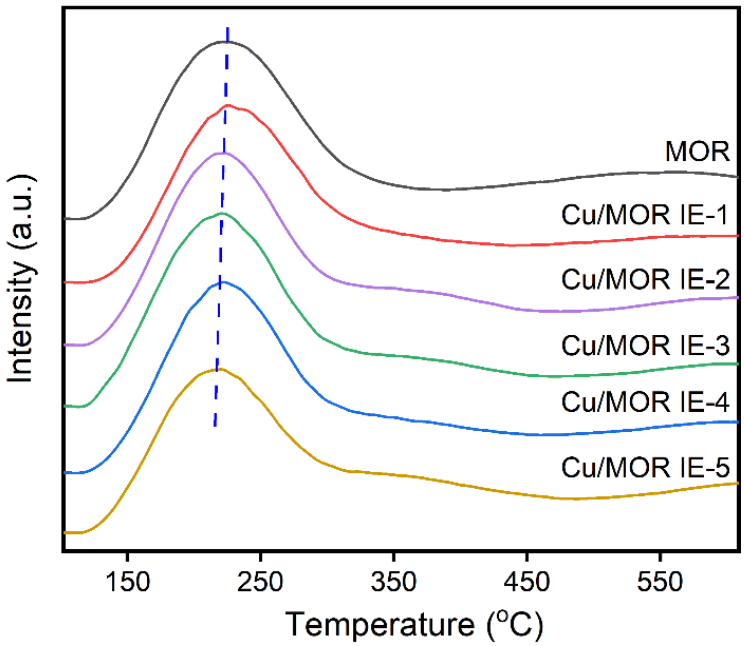

Figure S6. NH_3-TPD patterns of the fresh Cu/MOR catalysts with different exchange levels.

The acidity of the MOR and Cu-MOR samples was measured by NH_3 temperature programmed desorption (NH_3-TPD) and infrared spectroscopy of pyridine adsorption (Py-IR). The NH_3-TPD profile (Figure S6) shows simple MOR zeolites desorbing NH_3 in two different temperature ranges: a low temperature desorption range corresponding to weakly bound NH_3, and another high temperature range corresponding to relative strongly bound NH_3. The new desorption peak at around 320 °C after Cu ion exchange is attributed to NH_3 adsorption on sites of medium acidity, thus indicating the formation of new acidic sites, while strong acidic sites disappear and the central temperature of weak acidic sites shifts to lower temperatures, indicating weakening of the acidic strength.[11]

S10. Three experiments of Cu-MOR catalyst treated by different plasmas

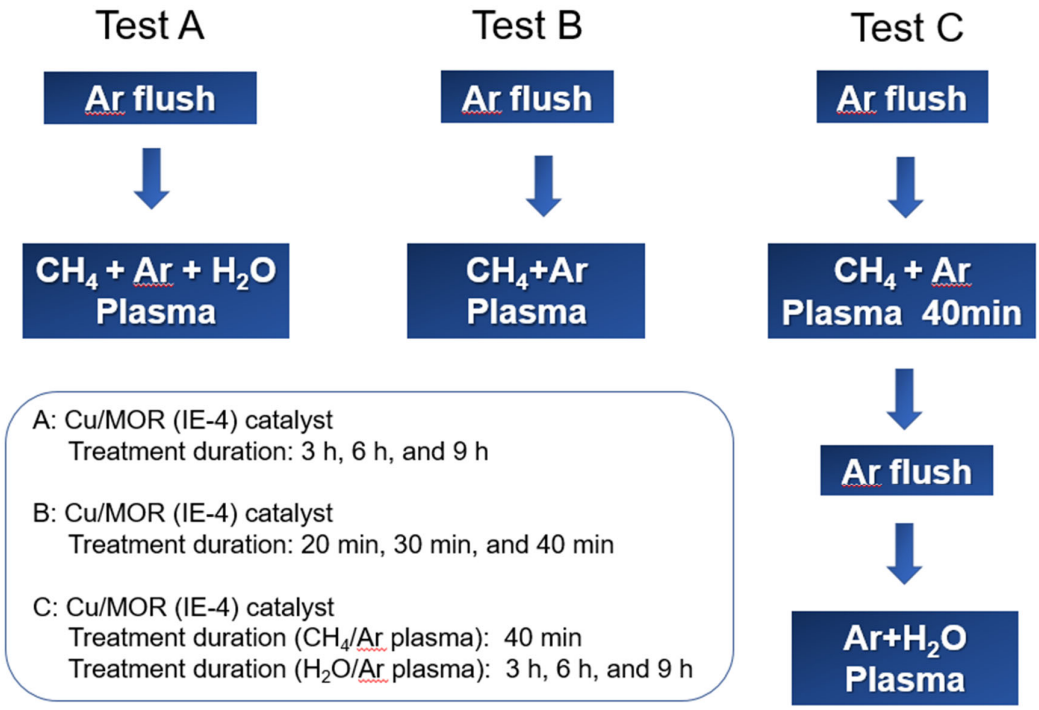

Figure S7. Diagram of Cu/MOR catalysts treated under different plasma conditions

S11. Lissajous plots under different conditions

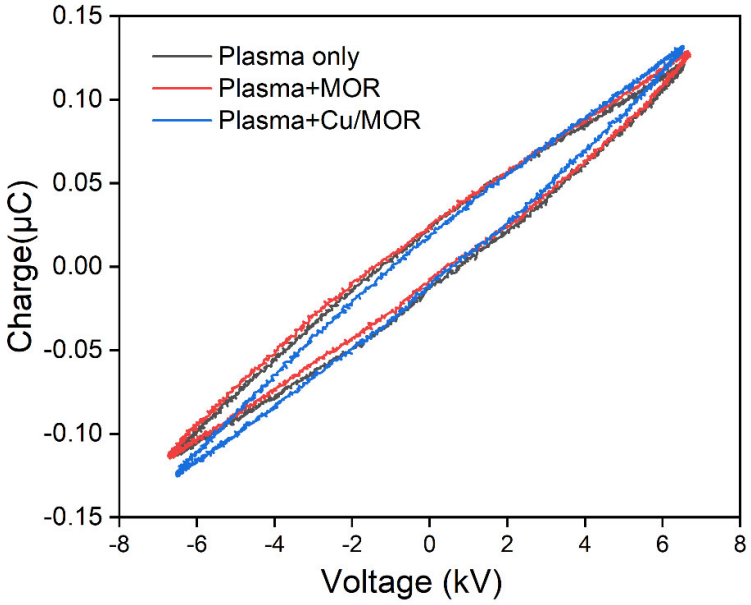

Figure S8. Lissajous plots for plasma only, plasma + MOR, and plasma + Cu/MOR at 443 K.

The Lissajous figures (Figure S8) of plasma, plasma + MOR and plasma + Cu/MOR were used to calculate the plasma power and monitor the discharge properties. There is no evident change in the Lissajous figures between plasma + MOR and plasma + Cu/MOR.

References

(1) Jeong, Y. R.; Jung, H.; Kang, J.; Han, J. W.; Park, E. D., Continuous synthesis of methanol from methane and steam over copper-mordenite. *ACS Catal.* **2021**, 11 (3), 1065-1070.

(2) Koishybay, A.; Shantz, D. F., Water is the oxygen source for methanol produced in partial oxidation of methane in a flow reactor over Cu-SSZ-13. *J. Am. Chem. Soc.* **2020**, 142, 11962-11966.

(3) Sun, L.; Wang, Y.; Wang, C.; Xie, Z.; Guan, N.; Li, L., Water-involved methane-selective catalytic oxidation by dioxygen over copper zeolites. *Chem* **2021**, 7, 1557-1568.

(4) Lee, S. H.; Kang, J. K.; Park, E. D., Continuous methanol synthesis directly from methane and steam over Cu(II)-exchanged mordenite. *Korean J. of Chem. Eng.* **2018**, 35, 2145-2149.

(5) Sushkevich, V. L.; Palagin, D.; Ranocchiari, M.; van Bokhoven, J. A., Selective anaerobic oxidation of methane enables direct synthesis of methanol. *Science* **2017**, 356, 523–527.

(6) Sushkevich, V. L.; Palagin, D.; van Bokhoven, J. A., The effect of the active-site structure on the activity of copper mordenite in the aerobic and anaerobic conversion of methane into methanol. *Angew. Chem. Int. Ed.* **2018**, 57, 8906-8910.

(7) Takayuki., T.; Iizuka, S., Conversion of methane to methanol by a low-pressure steam plasma. *J. Environ. Eng. Technol* **2013**, 2, 35-39.

(8) Okazaki, K.; Kishida, T.; Ogawa, K.; Nozaki, T., Direct conversion from methane to methanol for high efficiency energy system with exergy regeneration. *Energy Conv. Manag.* **2002**, 43, 1459–1468.

(9) Bi, W.; Tang, Y.; Li, X.; Dai, C.; Song, C.; Guo, X.; Ma, X., One-step direct conversion of methane to methanol with water in non-thermal plasma. *Commun. Chem.* **2022**, 5, 124.

(10) Tang, Y.; Cui, Y.; Ren, G.; Ma, K.; Ma, X.; Dai, C.; Song, C., One-step synthesis methanol and hydrogen of methanol and hydrogen from methane and water using non-thermal plasma and Cu-Mordenite catalyst. *Fuel Process. Technol.* **2023**, 224, 107722.

(11) Wang, S.; Guo, W.; Zhu, L.; Wang, H.; Qiu, K.; Cen, K., Methyl acetate synthesis from dimethyl ether carbonylation over mordenite modified by cation exchange. *J. Phys. Chem. C* **2014**, 119, 524-533.